A Field Theoretical Comparison of FDTD and TLM

Michael Krumpholz, *Member, IEEE*, Christian Huber, and Peter Russer, *Fellow, IEEE*

***Abstract*—A field theoretical derivation of the three-dimensional TLM method with expanded node and of the three-dimensional TLM method with asymmetrical condensed node is given. In the derivation, the Method of Moments is applied to Maxwell's equations. The wave amplitudes are related to the tangential field components at the boundaries of the TLM cell. The same approach is applied to derive the FDTD method from Maxwell's equations. A complete dispersion analysis is given for the two TLM methods as well as for the FDTD method.**

I. Introduction

SINCE the first publication by Johns and Beurle in 1971 [1], the transmission line matrix (TLM) method has evolved as an attractive and widely used method in electromagnetic field computation. Recently, a field theoretic foundation of the TLM method has been given. The two-dimensional TLM method [2] and the TLM method with symmetrical condensed node [3] have been derived by applying the Method of Moments [4] to Maxwell's equations [5]–[7]. In this paper, the same approach is applied in the derivation of the expanded TLM node [2] and the asymmetrical condensed TLM node [2], [8]. Furthermore, a complete dispersion analysis for these TLM methods is given. To demonstrate the close relationship between TLM and FDTD, we derive Yee's FDTD scheme with central difference approximations [9] by applying the Method of Moments to Maxwell's equations. Thus, together with [7], [10], this paper gives a comparison of the various TLM and FDTD schemes based on a rigorous derivation from Maxwell's theory.

In TLM, the electromagnetic field is represented by wave amplitudes instead of electric and magnetic field components. The correct mapping between the wave amplitudes and field components is described by the cell boundary mapping [7]. Wave amplitudes are related to transverse electric and magnetic field components. Therefore, at first, the introduction of wave amplitudes in three-dimensional space requires the introduction of any set of surfaces of reference defining tangential planes. The transverse electromagnetic field components are defined with respect to these tangential planes. The propagation of the wave pulses is normal to the tangential planes. The boundary of an elementary TLM cell is formed by the surfaces of reference. In each boundary surface separating two TLM cells, a sampling point for the tangential electric and magnetic field components is chosen. In the network model of TLM, in each sampling point, one port is assigned to each polarization. By this way, we assign an elementary multiport to each TLM cell. In the literature, this multiport is called the TLM node. In the following, we use the term TLM *cell* for the geometrical object we have defined in the continuous space, whereas the term TLM *node* is used for the abstract network model representing the relations between the wave amplitudes at the ports associated with the sampling points of a TLM cell.

Due to the discretization, FDTD and TLM exhibit deviations from the linear dispersion behavior. Furthermore also unphysical or spurious modes may occur. Such unphysical modes do not converge to solutions of Maxwell's equations. These effects impose limitations on the accuracy of field computation. In this paper, a systematic comparison of the dispersion behavior and the occurrence of unphysical modes is given for Yee's FDTD scheme and the TLM schemes for the expanded node and for the asymmetrical condensed node. The dispersion relations have already been calculated for various FDTD schemes [11], [12] and for some TLM schemes [10], [13], [14]. We use a general approach for the computation of the dispersion relations and the discussion of the spurious modes based on the state space representation of the discretized electromagnetic field [5]–[7], [15]. The dispersion relations of the FDTD and TLM schemes are calculated from the solutions of the eigenvalue problem in the field state space. We distinguish between physical and unphysical eigenvectors in the field state space. Only physical eigenvectors describe solutions of the FDTD or TLM scheme which converge to solutions of Maxwell's equations for frequencies approaching zero. The unphysical eigenvectors describe artifacts introduced by the discretization of Maxwell's equations.

II. Three-Dimensional FDTD

The finite-difference time domain (FDTD) method is a mathematical approach for the solution of partial differential equations [16]. The partial derivatives are simply replaced by finite differences. In 1966, Yee has given a FDTD scheme for the solution of Maxwell equations [9]. In the FDTD method, space and time are discretized with increments Δl and Δt, respectively. We derive Yee's FDTD scheme with central difference approximations [9] by applying the Method of Moments to Maxwell's equations. The field components are represented by a series of subdomain basis functions.

Manuscript received October 10, 1995; revised April 24, 1995. This work was supported by the Deutsche Forschungsgemeinschaft.

M. Krumpholz was with the Ferdinand-Braun-Institut für Höchstfrequenztechnik, 12489 Berlin, Germany. He is now with the Radiation Laboratory, EECS Department of the University of Michigan, Ann Arbor, MI 48109-2122 USA.

C. Huber is with the Ferdinand-Braun-Institut für Höchstfrequenztechnik, 12489 Berlin, Germany.

P. Russer is with the Ferdinand-Braun-Institut für Höchstfrequenztechnik, 12489 Berlin, Germany and with the Lehrstuhl für Hochfrequenztechnik, Technische Universität München, 80333 München, Germany.

IEEE Log Number 9412679.

0018–9480/95$04.00 © 1995 IEEE

As subdomain basis functions, we use pulse functions in space and time. The field expansions of the magnetic field components are shifted by half a discretization interval in space and time with respect to the field expansions of the electric field components. As test functions, according to Galerkin's method [4], we use pulse functions in space and time, too. For simplicity, we restrict our considerations to the free space.

A. The Derivation of FDTD Using the Method of Moments

Maxwell's equations

$$\nabla \times \mathbf{H} = \frac{1}{Z_0 c}\frac{\partial \mathbf{E}}{\partial t} \tag{1}$$

$$\nabla \times \mathbf{E} = -\frac{Z_0}{c}\frac{\partial \mathbf{H}}{\partial t} \tag{2}$$

with the wave propagation velocity $c = 1/\sqrt{\mu_0 \epsilon_0}$ and the wave impedance for the free space $Z_0 = \sqrt{\mu_0/\epsilon_0}$ may be written in Cartesian components as

$$\frac{\partial H_z}{\partial y} - \frac{\partial H_y}{\partial z} = \frac{1}{Z_0 c}\frac{\partial E_x}{\partial t} \tag{3}$$

$$\frac{\partial H_x}{\partial z} - \frac{\partial H_z}{\partial x} = \frac{1}{Z_0 c}\frac{\partial E_y}{\partial t} \tag{4}$$

$$\frac{\partial H_y}{\partial x} - \frac{\partial H_x}{\partial y} = \frac{1}{Z_0 c}\frac{\partial E_z}{\partial t} \tag{5}$$

$$\frac{\partial E_z}{\partial y} - \frac{\partial E_y}{\partial z} = -Z_0/c\frac{\partial H_x}{\partial t} \tag{6}$$

$$\frac{\partial E_x}{\partial z} - \frac{\partial E_z}{\partial x} = -Z_0/c\frac{\partial H_y}{\partial t} \tag{7}$$

$$\frac{\partial E_y}{\partial x} - \frac{\partial E_x}{\partial y} = -Z_0/c\frac{\partial H_z}{\partial t}. \tag{8}$$

We expand the field components in

$$\begin{aligned}
E_x(\vec{x}, t) &= \sum_{k,l,m,n=-\infty}^{+\infty} {}_kE^x_{l+1/2,m,n} \\
&\quad \cdot h_k(t)h_{l+1/2}(x)h_m(y)h_n(z) \\
E_y(\vec{x}, t) &= \sum_{k,l,m,n=-\infty}^{+\infty} {}_kE^y_{l,m+1/2,n} \\
&\quad \cdot h_k(t)h_l(x)h_{m+1/2}(y)h_n(z) \\
E_z(\vec{x}, t) &= \sum_{k,l,m,n=-\infty}^{+\infty} {}_kE^z_{l,m,n+1/2} \\
&\quad \cdot h_k(t)h_l(x)h_m(y)h_{n+1/2}(z) \\
H_x(\vec{x}, t) &= \sum_{k,l,m,n=-\infty}^{+\infty} {}_{k+1/2}H^x_{l,m+1/2,n+1/2} \\
&\quad \cdot h_{k+1/2}(t)h_l(x)h_{m+1/2}(y)h_{n+1/2}(z) \\
H_y(\vec{x}, t) &= \sum_{k,l,m,n=-\infty}^{+\infty} {}_{k+1/2}H^y_{l+1/2,m,n+1/2} \\
&\quad \cdot h_{k+1/2}(t)h_{l+1/2}(x)h_m(y)h_{n+1/2}(z) \\
H_z(\vec{x}, t) &= \sum_{k,l,m,n=-\infty}^{+\infty} {}_{k+1/2}H^z_{l+1/2,m+1/2,n} \\
&\quad \cdot h_{k+1/2}(t)h_{l+1/2}(x)h_{m+1/2}(y)h_n(z)
\end{aligned} \tag{9}$$

where ${}_kE^{\mu}_{l,m,n}$ and ${}_kH^{\mu}_{l,m,n}$ with $\mu = x, y, z$ are constant expansion coefficients. The indices l, m, n, and k are the discrete space and time indices related to the space and time coordinates via $x = l\Delta x$, $y = m\Delta y$, $z = n\Delta z$, and $t = k\Delta t$, where Δx, Δy, Δz, and Δt represent the space discretization interval in x-, y-, z-direction and the time discretization interval, respectively. The function $h_m(x)$ is defined by

$$h_m(x) = h\left(\frac{x}{\Delta x} - m\right) \tag{10}$$

with the rectangular pulse function

$$h(x) = \begin{cases} 1 & \text{for } |x| < 1/2 \\ 1/2 & \text{for } |x| = 1/2. \\ 0 & \text{for } |x| > 1/2 \end{cases} \tag{11}$$

We insert the field expansions in Maxwell's equations and sample the equations using pulse functions as test functions. We calculate

$$\int_{-\infty}^{+\infty} h_m(x)h_{m'}(x)\,dx = \delta_{m,m'}\,\Delta x \tag{12}$$

where $\delta_{m,m'}$ represents the Kronecker symbol

$$\delta_{m,m'} = \begin{cases} 1 & \text{for } m = m' \\ 0 & \text{for } m \neq m'. \end{cases} \tag{13}$$

Using

$$\int_{-\infty}^{+\infty} \delta(x - x_0)f(x)\,dx = f(x_0) \tag{14}$$

and

$$\frac{\partial h(x)}{\partial x} = \delta(x + 1/2) - \delta(x - 1/2) \tag{15}$$

yields

$$\int_{-\infty}^{+\infty} h_m(x)\frac{\partial h_{m'+1/2}(x)}{\partial x}\,dx = \delta_{m,m'} - \delta_{m,m'+1}. \tag{16}$$

As an example, we consider (3). Sampling $\partial E_x/\partial t$ yields

$$\begin{aligned}
&\iiint\int \frac{\partial E_x}{\partial t} h_{l+1/2}(x)h_m(y)h_n(z)h_{k+1/2}(t)\,dx\,dy\,dz\,dt \\
&\quad = \sum_{k',l',m',n'=-\infty}^{+\infty} {}_{k'}E^x_{l'+1/2,m',n'}\,\delta_{l,l'}\,\delta_{m,m'}\,\delta_{n,n'} \\
&\qquad \cdot \Delta x\Delta y\,\Delta z(\delta_{k',k+1} - \delta_{k',k}) \\
&\quad = \Delta x\Delta y\,\Delta z({}_{k+1}E^x_{l+1/2,m,n} - {}_kE^x_{l+1/2,m,n}).
\end{aligned} \tag{17}$$

Sampling the two other terms of (3) in the same way, we obtain

$$\begin{aligned}
&\Delta z\,\Delta t({}_{k+1/2}H^z_{l+1/2,m+1/2,n} - {}_{k+1/2}H^z_{l+1/2,m-1/2,n}) \\
&\quad - \Delta y\,\Delta t({}_{k+1/2}H^y_{l+1/2,m,n+1/2} - {}_{k+1/2}H^x_{l+1/2,m,n-1/2}) \\
&\quad = \frac{\Delta y\,\Delta z}{Z_0 c}({}_{k+1}E^x_{l+1/2,m,n} - {}_kE^x_{l+1/2,m,n}).
\end{aligned} \tag{18}$$

Choosing

$$\Delta x = \Delta y = \Delta z = \Delta l \tag{19}$$

and proceeding in the same way as above with all components of Maxwell's equations yields Yee's FDTD scheme with central difference approximations [9]

$$
\begin{aligned}
&{}_{k+1}E^x_{l+1/2,m,n} - {}_kE^x_{l+1/2,m,n} \\
&\quad = sZ_0({}_{k+1/2}H^z_{l+1/2,m+1/2,n} - {}_{k+1/2}H^z_{l+1/2,m-1/2,n} \\
&\qquad + {}_{k+1/2}H^y_{l+1/2,m,n-1/2} - {}_{k+1/2}H^y_{l+1/2,m,n+1/2}) \\
&{}_{k+1}E^y_{l,m+1/2,n} - {}_kE^y_{l,m+1/2,n} \\
&\quad = sZ_0({}_{k+1/2}H^x_{l,m+1/2,n+1/2} - {}_{k+1/2}H^x_{l,m+1/2,n-1/2} \\
&\qquad + {}_{k+1/2}H^z_{l-1/2,m+1/2,n} - {}_{k+1/2}H^z_{l+1/2,m+1/2,n}) \\
&{}_{k+1}E^z_{l,m,n+1/2} - {}_kE^z_{l,m,n+1/2} \\
&\quad = sZ_0({}_{k+1/2}H^x_{l,m-1/2,n+1/2} - {}_{k+1/2}H^x_{l,m+1/2,n+1/2} \\
&\qquad + {}_{k+1/2}H^y_{l+1/2,m,n+1/2} - {}_{k+1/2}H^y_{l-1/2,m,n+1/2}) \\
&{}_{k+1/2}H^x_{l,m+1/2,n+1/2} - {}_{k-1/2}H^x_{l,m+1/2,n+1/2} \\
&\quad = \frac{s}{Z_0}({}_kE^y_{l,m+1/2,n+1} - {}_kE^y_{l,m+1/2,n} \\
&\qquad + {}_kE^z_{l,m,n+1/2} - {}_kE^z_{l,m+1,n+1/2}) \\
&{}_{k+1/2}H^y_{l+1/2,m,n+1/2} - {}_{k-1/2}H^y_{l+1/2,m,n+1/2} \\
&\quad = \frac{s}{Z_0}({}_kE^x_{l+1/2,m,n} - {}_kE^x_{l+1/2,m,n+1} \\
&\qquad + {}_kE^z_{l+1,m,n+1/2} - {}_kE^z_{l,m,n+1/2}) \\
&{}_{k+1/2}H^z_{l+1/2,m+1/2,n} - {}_{k-1/2}H^z_{l+1/2,m+1/2,n} \\
&\quad = \frac{s}{Z_0}({}_kE^x_{l+1/2,m+1,n} - {}_kE^x_{l+1/2,m,n} \\
&\qquad + {}_kE^y_{l,m+1/2,n} - {}_kE^y_{l+1,m+1/2,n})
\end{aligned} \tag{20}
$$

where we have introduced the stability factor $s = c\Delta t/\Delta l$.

To write these discretized field equations in a more compact form, we use the state space representation for the electromagnetic field presented in [5]–[7], [15]. We introduce the field state space $\mathcal{H}_F$ given by the product space of three vectors spaces

$$\mathcal{H}_F = \mathcal{C}^6 \otimes \mathcal{H}_m \otimes \mathcal{H}_t \tag{21}$$

and define the field vector $|F\rangle$ as a vector in $\mathcal{H}_F$

$$
\begin{aligned}
|F\rangle = \sum_{k,l,m,n=-\infty}^{+\infty} {}_k[&E_x,\, E_y,\, E_z,\, Z_0H_x, \\
&Z_0H_y,\, Z_0H_z]^T_{l,m,n}\, |k;\, l,\, m,\, n\rangle.
\end{aligned} \tag{22}
$$

The six-dimensional complex vector space $\mathcal{C}^6$ is the space of the vector ${}_k[E_x,\, E_y,\, E_z,\, Z_0H_x,\, Z_0H_y,\, Z_0H_z]^T_{l,m,n}$ combining the six field components of the FDTD cell with the discrete coordinates $(l,\, m,\, n)$ at the discrete time coordinate k. We introduce a system of orthonormal space domain basis vectors $|l,\, m,\, n\rangle$ in the Hilbert space $\mathcal{H}_m$. To each node with the discrete coordinates $(l,\, m,\, n)$, a basis vector $|l,\, m,\, n\rangle$ is assigned. In the Hilbert space $\mathcal{H}_t$, the basis vector $|k\rangle$ corresponds to the discrete time coordinate k. Due to the summation of k, l, m and n, the field vector $|F\rangle$ combines all electric and magnetic field components of the complete FDTD mesh at all discrete time points k. Thus the complete time evolution of the field in four-dimensional space-time may be represented by a single vector in $\mathcal{H}_F$.

The orthonormal basis vectors of $\mathcal{H}_m \otimes \mathcal{H}_t$ are given by the ket-vectors $|k;\, l,\, m,\, n\rangle$. The bra-vector $\langle k;\, l,\, m,\, n|$ is the Hermitian conjugate of $|k;\, l,\, m,\, n\rangle$. The orthogonality relations are given by

$$
\begin{aligned}
&\langle k_1;\, l_1,\, m_1,\, n_1\, |k_2;\, l_2,\, m_2,\, n_2\rangle \\
&\qquad = \delta_{k_1,k_2}\, \delta_{l_1,l_2}\, \delta_{m_1,m_2}\, \delta_{n_1,n_2}.
\end{aligned} \tag{23}
$$

To describe a shift of the field components in space and time, we define the half shift operators $\boldsymbol{X}_h$ and its Hermitian conjugate $\boldsymbol{X}_h^\dagger$ by

$$
\begin{aligned}
\boldsymbol{X}_h\, |k;\, l,\, m,\, n\rangle &= |k;\, l + 1/2,\, m,\, n\rangle \\
\boldsymbol{X}_h^\dagger\, |k;\, l,\, m,\, n\rangle &= |k;\, l - 1/2,\, m,\, n\rangle
\end{aligned} \tag{24}
$$

and in the same way, the shift operators $\boldsymbol{Y}_h$, $\boldsymbol{Y}_h^\dagger$, $\boldsymbol{Z}_h$, and $\boldsymbol{Z}_h^\dagger$ for the spatial coordinates m and n as well as the half time shift operators $\boldsymbol{T}_h$ and $\boldsymbol{T}_h^\dagger$ for the time coordinate k. Using the Hilbert space representation, we may represent (20) by the operator equation

$$\boldsymbol{M}\, |F\rangle = 0 \tag{25}$$

with (26), shown at the bottom of the page, where we have used the abbreviations

$$
\begin{aligned}
\boldsymbol{d}_x &= \boldsymbol{X}_h^\dagger - \boldsymbol{X}_h \\
\boldsymbol{d}_y &= \boldsymbol{Y}_h^\dagger - \boldsymbol{Y}_h \\
\boldsymbol{d}_z &= \boldsymbol{Z}_h^\dagger - \boldsymbol{Z}_h \\
\boldsymbol{d}_t &= \boldsymbol{T}_h^\dagger - \boldsymbol{T}_h.
\end{aligned} \tag{27}
$$

$$
\boldsymbol{M} = \begin{bmatrix}
\frac{1}{s}\boldsymbol{X}_h^\dagger \boldsymbol{T}_h^\dagger \boldsymbol{d}_t^\dagger & 0 & 0 & 0 & \boldsymbol{T}_h^\dagger \boldsymbol{X}_h^\dagger \boldsymbol{d}_z^\dagger & \boldsymbol{T}_h^\dagger \boldsymbol{X}_h^\dagger \boldsymbol{d}_y \\
0 & \frac{1}{s}\boldsymbol{Y}_h^\dagger \boldsymbol{T}_h^\dagger \boldsymbol{d}_t^\dagger & 0 & \boldsymbol{T}_h^\dagger \boldsymbol{Y}_h^\dagger \boldsymbol{d}_z & 0 & \boldsymbol{T}_h^\dagger \boldsymbol{Y}_h^\dagger \boldsymbol{d}_x^\dagger \\
0 & 0 & \frac{1}{s}\boldsymbol{Z}_h^\dagger \boldsymbol{T}_h^\dagger \boldsymbol{d}_t^\dagger & \boldsymbol{T}_h^\dagger \boldsymbol{Z}_h^\dagger \boldsymbol{d}_y^\dagger & \boldsymbol{T}_h^\dagger \boldsymbol{Z}_h^\dagger \boldsymbol{d}_x & 0 \\
0 & \boldsymbol{Y}_h^\dagger \boldsymbol{Z}_h^\dagger \boldsymbol{d}_z & \boldsymbol{Y}_h^\dagger \boldsymbol{Z}_h^\dagger \boldsymbol{d}_y^\dagger & \frac{1}{s}\boldsymbol{Y}_h^\dagger \boldsymbol{Z}_h^\dagger \boldsymbol{d}_t^\dagger & 0 & 0 \\
\boldsymbol{X}_h^\dagger \boldsymbol{Z}_h^\dagger \boldsymbol{d}_z^\dagger & 0 & \boldsymbol{X}_h^\dagger \boldsymbol{Z}_h^\dagger \boldsymbol{d}_x & 0 & \frac{1}{s}\boldsymbol{X}_h^\dagger \boldsymbol{Z}_h^\dagger \boldsymbol{d}_t^\dagger & 0 \\
\boldsymbol{X}_h^\dagger \boldsymbol{Y}_h^\dagger \boldsymbol{d}_y & \boldsymbol{X}_h^\dagger \boldsymbol{Y}_h^\dagger \boldsymbol{d}_x^\dagger & 0 & 0 & 0 & \frac{1}{s}\boldsymbol{X}_h^\dagger \boldsymbol{Y}_h^\dagger \boldsymbol{d}_t^\dagger
\end{bmatrix} \tag{26}
$$

B. The Dispersion Analysis

The dispersion characteristics of FDTD have already been investigated extensively in [10]–[12] so that we only summarize the results which are necessary for the comparison of FDTD and TLM. We introduce a set of basis vectors $|\Omega\rangle$ of $\mathcal{H}_t$

$$|\Omega\rangle = \sum_{k=-\infty}^{+\infty} e^{jk\Omega} |k\rangle \tag{28}$$

where the normalized frequency Ω is related to the frequency f by $\Omega = 2\pi\Delta t f = \omega\Delta t$. Calculating the inner product of $|F\rangle$ and $|\Omega\rangle$ yields the frequency domain representation of the field state [10], [14]. Forming the inner product of $\langle\Omega|$ and (25) and considering

$$\boldsymbol{T}_h |\Omega;\, l,\, m,\, n\rangle = e^{-j\Omega/2} |\Omega;\, l,\, m,\, n\rangle \tag{29}$$

we obtain

$$\boldsymbol{M}(e^{-j\Omega/2},\, \boldsymbol{X}_h,\, \boldsymbol{Y}_h,\, \boldsymbol{Z}_h)\, |F(\Omega)\rangle_m = 0 \tag{30}$$

where we have introduced the vector

$$\begin{aligned} |F(\Omega)\rangle_m &= {}_t\langle\Omega\,|\,F\rangle \\ &= \sum_{l,\,m,\,n=-\infty}^{+\infty} {}_k[E_x,\, E_y,\, E_z,\, Z_0H_x, \\ &\quad Z_0H_y,\, Z_0H_z]^T_{l,\,m,\,n} e^{-jk\Omega} |l,\, m,\, n\rangle. \end{aligned} \tag{31}$$

The subscripts t and m of the vectors indicate that the vectors are an element of the Hilbert space $\mathcal{H}_t$ and $\mathcal{H}_m$, respectively. If it is obvious to which space the vectors are belonging, these indices will be omitted. The procedure corresponds to a separation of variables, which is justified because $|\Omega\rangle$ represents a maximal orthonormal set for the Hilbert space $\mathcal{H}_t$ [17].

We introduce the plane wave basis vectors

$$|\chi,\, \eta,\, \xi\rangle = \sum_{l,\,m,\,n=-\infty}^{+\infty} e^{j(\chi l+\eta m+\xi n)} |l,\, m,\, n\rangle \tag{32}$$

with the normalized wave vector components $\chi = \Delta l\, k_x$, $\eta = \Delta l\, k_y$, and $\xi = \Delta l\, k_z$. The wave vector $\vec{k}$ has the x-, y-, and z-components k_x, k_y, and k_z. The basis vectors $|\chi,\, \eta,\, \xi\rangle$ form a complete basis in $\mathcal{H}_m$ satisfying the completeness relation

$$\int_0^{2\pi}\int_0^{2\pi}\int_0^{2\pi} d\chi\, d\eta\, d\xi\, |\chi,\, \eta,\, \xi\rangle\, \langle\chi,\, \eta,\, \xi| = 1. \tag{33}$$

Therefore (22) yields

$$\begin{aligned} |F(\Omega)\rangle_m = \int_0^{2\pi}\int_0^{2\pi}\int_0^{2\pi} d\chi\, d\eta\, d\xi\, \vec{F}(\chi,\, \eta,\, \xi) \\ \cdot e^{-jk\Omega} |\chi,\, \eta,\, \xi\rangle \end{aligned} \tag{34}$$

where we have introduced the vector of the plane wave amplitudes

$$\begin{aligned} \vec{F}(\chi,\, \eta,\, \xi) = \sum_{l,\,m,\,n=-\infty}^{+\infty} {}_k[E_x,\, E_y,\, E_z,\, Z_0H_x, \\ Z_0H_y,\, Z_0H_z]^T_{l,\,m,\,n}\, e^{-j(\chi l+\eta m+\xi n)}. \end{aligned} \tag{35}$$

We restrict our investigations to electromagnetic fields composed of plane waves. In this case, we have

$$|F(\Omega)\rangle_m = \vec{F}(\chi,\, \eta,\, \xi) e^{-jk\Omega} |\chi,\, \eta,\, \xi\rangle \tag{36}$$

and (30) yields

$$\boldsymbol{M}(e^{-j\Omega/2},\, \boldsymbol{X}_h,\, \boldsymbol{Y}_h,\, \boldsymbol{Z}_h)\vec{F}(\chi,\, \eta,\, \xi)\, |\chi,\, \eta,\, \xi\rangle = 0. \tag{37}$$

We calculate the inner product of $\langle\chi,\, \eta,\, \xi|$ and (37). Considering

$$\begin{aligned} \boldsymbol{X}_h |\chi,\, \eta,\, \xi\rangle &= e^{-j\chi/2} |\chi,\, \eta,\, \xi\rangle \\ \boldsymbol{Y}_h |\chi,\, \eta,\, \xi\rangle &= e^{-j\eta/2} |\chi,\, \eta,\, \xi\rangle \\ \boldsymbol{Z}_h |\chi,\, \eta,\, \xi\rangle &= e^{-j\xi/2} |\chi,\, \eta,\, \xi\rangle \end{aligned} \tag{38}$$

we obtain the representation of (37) in wave vector domain

$$\boldsymbol{M}(e^{-j\Omega/2},\, e^{-j\chi/2},\, e^{-j\eta/2},\, e^{-j\xi/2})\, \vec{F}(\chi,\, \eta,\, \xi) = 0. \tag{39}$$

Equation (39) has nontrivial solutions if

$$\det \boldsymbol{M}(e^{-j\Omega/2},\, e^{-j\chi/2},\, e^{-j\eta/2},\, e^{-j\xi/2}) = 0. \tag{40}$$

The solutions of (40) are the eigenvalues $\lambda_\iota = e^{j\Omega_\iota}$ given by

$$\begin{aligned} \lambda_{1,\,2} &= C_1 + \sqrt{(C_1)^2 - 1} \\ \lambda_{3,\,4} &= C_1 - \sqrt{(C_1)^2 - 1} \\ \lambda_{5,\,6} &= 1 \end{aligned} \tag{41}$$

with

$$C_1 = s^2[\cos(\chi) + \cos(\eta) + \cos(\xi) - 3] + 1. \tag{42}$$

Each of the six eigenvalues λ_ι has one eigenvector $\vec{F}_\iota(\chi,\, \eta,\, \xi)$. The eigenvectors corresponding to the eigenvalues λ_1, λ_2, λ_3, and λ_4 describe propagating solutions of the FDTD scheme. As $\lambda_{5,\,6} = 1$ implies $\Omega = 0$, the corresponding eigenvectors describe stationary solutions representing the electro- and magnetostatic case.

For the eigenvectors describing propagating solutions of the FDTD scheme, we obtain the dispersion relation

$$\sin^2(\Omega/2) = s^2[(\sin^2(\chi/2) + \sin^2(\eta/2) + \sin^2(\xi/2)]. \tag{43}$$

To compare three-dimensional FDTD with three-dimensional TLM, we choose $s = 1/2$. For this case, we calculate the cutoff frequencies. The cutoff frequency is defined as the highest frequency for which a solution of the dispersion relation exists. The cutoff frequency is the highest frequency for which the propagation of a wave with an arbitrary spatial distribution in the FDTD mesh is still possible. For example, for wave propagation along the x-axis and in (1, 0, 0) direction, respectively, we have $\eta = 0$ and $\xi = 0$ yielding

$$\sin(\Omega/2) \le \frac{1}{2} \quad \text{and} \quad f_c = \frac{1}{6\Delta t} \tag{44}$$

for the cutoff frequency f_c. For wave propagation along the space diagonal with respect to the mesh and in (1, 1, 1) direction, respectively, we have $\chi = \eta = \xi$ yielding

$$\sin(\Omega/2) \le \frac{\sqrt{3}}{2} \quad \text{and} \quad f_c = \frac{1}{3\Delta t}. \tag{45}$$

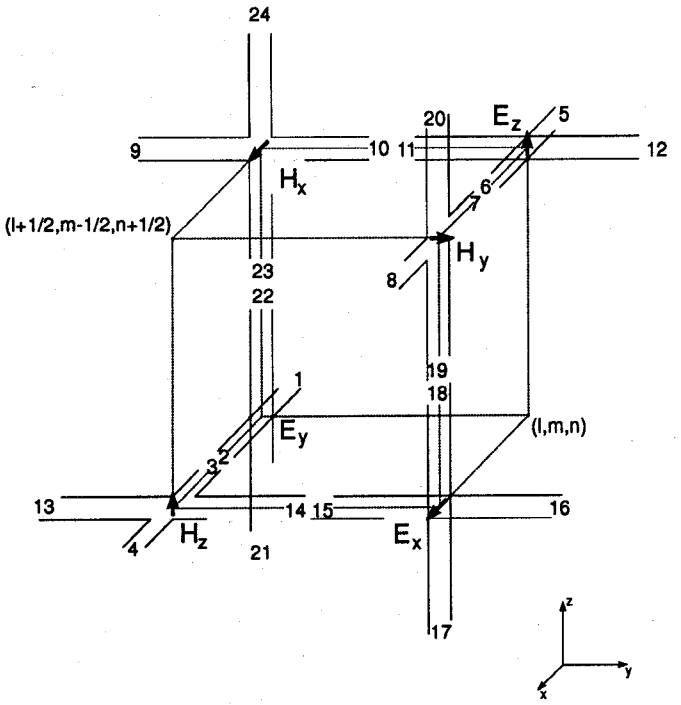

Fig. 1. The three-dimensional expanded TLM node.

The lowest cutoff frequency determines the maximum bandwidth with respect to frequency. Thus the maximum bandwidth F of the FDTD method is given by $-1/(6\Delta t) \leq f \leq 1/(6\Delta t)$ and $F = 1/(3\Delta t)$, respectively.

III. The TLM Method with Expanded Node

The expanded TLM node (Fig. 1) is composed of three two-dimensional TLM shunt nodes and three two-dimensional TLM series nodes [2]. The scattering at the shunt nodes is shifted by half a discretization interval in time with respect to the scattering at the series nodes. The scattering of the wave amplitudes at the expanded TLM node may be described by two 12×12-matrices combining the scattering matrices of the three shunt nodes in one 12×12-matrix and the scattering matrices of the three series nodes in the other 12×12-matrix. The field expansions of the electric and magnetic field components are similar to the field expansions for the derivation of the FDTD method. Like in FDTD, the field expansions of the magnetic field components are shifted by half a discretization interval in space and time with respect to the field expansions of the electric field components. Thus each of the six linearly independent electric and magnetic field components per three-dimensional TLM cell is defined at the center of one of the six two-dimensional TLM nodes of one expanded node. In the following, we derive the scattering matrix of one shunt node of the expanded TLM node. The other five scattering matrices may be derived in a similar way.

A. Field Theoretic Derivation

We expand the field components in

$$E_x(\vec{x}, t) = \sum_{k,l,m,n=-\infty}^{+\infty} {}_kE^x_{l+1/2,m,n} g_k(t) \cdot h_{l+1/2}(x) g_m(y) g_n(z)$$

$$E_y(\vec{x}, t) = \sum_{k,l,m,n=-\infty}^{+\infty} {}_kE^y_{l,m+1/2,n} g_k(t) \cdot g_l(x) h_{m+1/2}(y) g_n(z)$$

$$E_z(\vec{x}, t) = \sum_{k,l,m,n=-\infty}^{+\infty} {}_kE^z_{l,m,n+1/2} g_k(t) \cdot g_l(x) g_m(y) h_{n+1/2}(z)$$

$$H_x(\vec{x}, t) = \sum_{k,l,m,n=-\infty}^{+\infty} {}_{k+1/2}H^x_{l,m+1/2,n+1/2} \cdot g_{k+1/2}(t) h_l(x) g_{m+1/2}(y) g_{n+1/2}(z)$$

$$H_y(\vec{x}, t) = \sum_{k,l,m,n=-\infty}^{+\infty} {}_{k+1/2}H^y_{l+1/2,m,n+1/2} \cdot g_{k+1/2}(t) g_{l+1/2}(x) h_m(y) g_{n+1/2}(z)$$

$$H_z(\vec{x}, t) = \sum_{k,l,m,n=-\infty}^{+\infty} {}_{k+1/2}H^z_{l+1/2,m+1/2,n} \cdot g_{k+1/2}(t) g_{l+1/2}(x) g_{m+1/2}(y) h_n(z). \quad (46)$$

The basis functions g_m are given by

$$g_m(x) = g\left(\frac{x}{\Delta x} - m\right) \quad (47)$$

where the triangle function $g(x)$ is defined by

$$g(x) = \begin{cases} 1 - |x| & \text{for } |x| < 1 \\ 0 & \text{for } |x| \geq 1 \end{cases}. \quad (48)$$

The use of the functions $g_m(x)$ provides a piecewise linear approximation [4] of the exact solution of Maxwell's equations with respect to the coordinate x, whereas the use of the pulse functions $h_m(x')$ provides a step approximation [4] of the exact solution with respect to the coordinate x'.

For the derivation of the two-dimensional shunt node with the center at the discrete space point $(l, m, n + 1/2)$ (see Fig. 1), we insert the field expansions in Maxwell equations and sample the equations in the cell boundaries using delta functions in space and time. Sampling (5) in the cell boundaries means sampling it at $(l + 1/4, m, n + 1/2)$, $(l - 1/4, m, n+1/2)$, $(l, m+1/4, n+1/2)$, and $(l, m-1/4, n+1/2)$ at the discrete time points $k+1/4$ and $k+3/4$. We choose Δl according to (19). Using the integrals

$$\int_{-\infty}^{+\infty} \delta[x - (m + \epsilon)\Delta x] h_{m'}(x)\, dx = \delta_{m,m'} \quad (49)$$

$$\int_{-\infty}^{+\infty} \delta(x - m\Delta x) g_{m'}(x)\, dx = \delta_{m,m'} \quad (50)$$

$$\int_{-\infty}^{+\infty} \delta[x - (m + 1/4)\Delta x] g_{m'}(x)\, dx = \tfrac{1}{4}(3\,\delta_{m,m'} + \delta_{m+1,m'}) \quad (51)$$

$$\int_{-\infty}^{+\infty} \delta[x - (m + 3/4)\Delta x] g_{m'}(x)\, dx = \tfrac{1}{4}(\delta_{m,m'} + 3\,\delta_{m+1,m'}) \quad (52)$$

$$\int_{-\infty}^{+\infty} \delta[x-(m+1/2+\epsilon)\Delta x]\,\frac{\partial g_{m'}(x)}{\partial x}\,dx = \delta_{m+1,\,m'} - \delta_{m,\,m'} \tag{53}$$

for $\epsilon = -1/4,\ 0,\ 1/4$, we obtain eight discretized field equations. Adding these discretized field equations yields

$$\begin{aligned}
&12\,{}_{k+1}E^z_{l,\,m,\,n+1/2} + {}_{k+1}E^z_{l+1,\,m,\,n+1/2} \\
&\quad + {}_{k+1}E^z_{l-1,\,m,\,n+1/2} + {}_{k+1}E^z_{l,\,m+1,\,n+1/2} \\
&\quad + {}_{k+1}E^z_{l,\,m-1,\,n+1/2} - 12\,{}_{k}E^z_{l,\,m,\,n+1/2} \\
&\quad - {}_{k}E^z_{l+1,\,m,\,n+1/2} - {}_{k}E^z_{l-1,\,m,\,n+1/2} \\
&\quad - {}_{k}E^z_{l,\,m+1,\,n+1/2} - {}_{k}E^z_{l,\,m-1,\,n+1/2} \\
&\qquad = Z\eta_1({}_{k+3/2}H^y_{l+1/2,\,m,\,n+1/2} \\
&\qquad\quad + 6\,{}_{k+1/2}H^y_{l+1/2,\,m,\,n+1/2} \\
&\qquad\quad + {}_{k-1/2}H^y_{l+1/2,\,m,\,n+1/2}) \\
&\qquad\quad - Z\eta_1({}_{k+3/2}H^y_{l-1/2,\,m,\,n+1/2} \\
&\qquad\quad + 6\,{}_{k+1/2}H^y_{l-1/2,\,m,\,n+1/2} \\
&\qquad\quad + {}_{k-1/2}H^y_{l-1/2,\,m,\,n+1/2}) \\
&\qquad\quad - Z\eta_1({}_{k+3/2}H^x_{l,\,m+1/2,\,n+1/2} \\
&\qquad\quad + 6\,{}_{k+1/2}H^x_{l,\,m+1/2,\,n+1/2} \\
&\qquad\quad + {}_{k-1/2}H^x_{l,\,m+1/2,\,n+1/2}) \\
&\qquad\quad + Z\eta_1({}_{k+3/2}H^x_{l,\,m-1/2,\,n+1/2} \\
&\qquad\quad + 6\,{}_{k+1/2}H^x_{l,\,m-1/2,\,n+1/2} \\
&\qquad\quad + {}_{k-1/2}H^x_{l,\,m-1/2,\,n+1/2})
\end{aligned} \tag{54}$$

where we have introduced

$$\eta_1 = \frac{2Z_0\Delta tc}{Z\Delta l} \tag{55}$$

with the arbitrary impedance Z.

The correct mapping between the wave amplitudes and field components is described by the cell boundary mapping [7]. The cell boundary mapping relates the wave amplitudes with the tangential electric and magnetic field components in the boundary surfaces separating the six two-dimensional TLM nodes of one expanded node. For the field components at the cell boundaries, we introduce the CBM values (cell boundary mean values [5]) of the electric and magnetic field components. The CBM value of a field component is defined as the value of the series expansion for this field component at the cell boundary. We introduce the CBM values of the z-component of the electric field

$$\begin{aligned}
&{}_{k}E^z_{l+1/4,\,m,\,n+1/2} = \tfrac{1}{4}({}_{k}E^z_{l+1,\,m,\,n+1/2} + 3\,{}_{k}E^z_{l,\,m,\,n+1/2}) \\
&{}_{k}E^z_{l-1/4,\,m,\,n+1/2} = \tfrac{1}{4}({}_{k}E^z_{l-1,\,m,\,n+1/2} + 3\,{}_{k}E^z_{l,\,m,\,n+1/2}) \\
&{}_{k}E^z_{l,\,m+1/4,\,n+1/2} = \tfrac{1}{4}({}_{k}E^z_{l,\,m+1,\,n+1/2} + 3\,{}_{k}E^z_{l,\,m,\,n+1/2}) \\
&{}_{k}E^z_{l,\,m-1/4,\,n+1/2} = \tfrac{1}{4}({}_{k}E^z_{l,\,m-1,\,n+1/2} + 3\,{}_{k}E^z_{l,\,m,\,n+1/2})
\end{aligned} \tag{56}$$

and the CBM values of the x- and y-component of the magnetic field

$$\begin{aligned}
&{}_{k+1/2}H^x_{l,\,m+1/4,\,n+1/2} = \tfrac{1}{4}(3\,{}_{k+1/2}H^x_{l,\,m+1/2,\,n+1/2} + {}_{k+1/2}H^x_{l,\,m-1/2,\,n+1/2}) \\
&{}_{k+1/2}H^x_{l,\,m-1/4,\,n+1/2} = \tfrac{1}{4}({}_{k+1/2}H^x_{l,\,m+1/2,\,n+1/2} + 3\,{}_{k+1/2}H^x_{l,\,m-1/2,\,n+1/2}) \\
&{}_{k+1/2}H^y_{l+1/4,\,m,\,n+1/2} = \tfrac{1}{4}(3\,{}_{k+1/2}H^y_{l+1/2,\,m,\,n+1/2} + {}_{k+1/2}H^y_{l-1/2,\,m,\,n+1/2}) \\
&{}_{k+1/2}H^y_{l-1/4,\,m,\,n+1/2} = \tfrac{1}{4}({}_{k+1/2}H^y_{l+1/2,\,m,\,n+1/2} + 3\,{}_{k+1/2}H^y_{l-1/2,\,m,\,n+1/2}).
\end{aligned} \tag{57}$$

Furthermore, we introduce the CBM values of the field components with respect to time as

$$\begin{aligned}
&{}_{k+1/4}E^z_{l,\,m,\,n} = \tfrac{1}{4}({}_{k+1}E^z_{l,\,m,\,n} + 3\,{}_{k}E^z_{l,\,m,\,n}) \\
&{}_{k+3/4}E^z_{l,\,m,\,n} = \tfrac{1}{4}(3\,{}_{k+1}E^z_{l,\,m,\,n} + {}_{k}E^z_{l,\,m,\,n}) \\
&{}_{k+1/4}H^\mu_{l,\,m,\,n} = \tfrac{1}{4}(3\,{}_{k+1/2}H^\mu_{l,\,m,\,n} + {}_{k-1/2}H^\mu_{l,\,m,\,n}) \\
&{}_{k+3/4}H^\mu_{l,\,m,\,n} = \tfrac{1}{4}({}_{k+3/2}H^\mu_{l,\,m,\,n} + 3\,{}_{k+1/2}H^\mu_{l,\,m,\,n}).
\end{aligned} \tag{58}$$

with $\mu = x,\ y$. Inserting (56)–(58) in (54) yields

$$\begin{aligned}
&{}_{k+3/4}E^z_{l+1/4,\,m,\,n+1/2} + {}_{k+3/4}E^z_{l-1/4,\,m,\,n+1/2} \\
&\quad + {}_{k+3/4}E^z_{l,\,m+1/4,\,n+1/2} + {}_{k+3/4}E^z_{l,\,m-1/4,\,n+1/2} \\
&\quad - {}_{k+1/4}E^z_{l+1/4,\,m,\,n+1/2} - {}_{k+1/4}E^z_{l-1/4,\,m,\,n+1/2} \\
&\quad - {}_{k+1/4}E^z_{l,\,m+1/4,\,n+1/2} - {}_{k+1/4}E^z_{l,\,m-1/4,\,n+1/2} \\
&\qquad = Z\eta_1({}_{k+3/4}H^y_{l+1/4,\,m,\,n+1/2} \\
&\qquad\quad + {}_{k+1/4}H^y_{l+1/4,\,m,\,n+1/2} \\
&\qquad\quad - {}_{k+3/4}H^y_{l-1/4,\,m,\,n+1/2} \\
&\qquad\quad - {}_{k+1/4}H^y_{l-1/4,\,m,\,n+1/2}) \\
&\qquad\quad - Z\eta_1({}_{k+3/4}H^x_{l,\,m+1/4,\,n+1/2} \\
&\qquad\quad + {}_{k+1/4}H^x_{l,\,m+1/4,\,n+1/2} \\
&\qquad\quad - {}_{k+3/4}H^x_{l,\,m-1/4,\,n+1/2} \\
&\qquad\quad - {}_{k+1/4}H^x_{l,\,m-1/4,\,n+1/2}).
\end{aligned} \tag{59}$$

In order to describe the complete discretized mesh-state, we make use of the Hilbert space representation of the TLM method [15] and introduce the field state space $\mathcal{H}_W$ given by

$$\mathcal{H}_W = \mathcal{C}^{12} \otimes \mathcal{H}_m \otimes \mathcal{H}_t. \tag{60}$$

The electric field vector $|F_{E1}\rangle$ combines all CBM values of the electric field components at the three shunt nodes of all

expanded TLM nodes of the three-dimensional mesh at all time sampling points $k\Delta t$. It is given by

$$|F_{E1}\rangle = \sum_{k,l,m,n=-\infty}^{+\infty} \begin{bmatrix} {}_{k+3/4}E^{y}_{l-1/4,m-1/2,n} \\ {}_{k+3/4}E^{y}_{l+1/4,m-1/2,n} \\ {}_{k+3/4}E^{z}_{l-1/4,m,n+1/2} \\ {}_{k+3/4}E^{z}_{l+1/4,m,n+1/2} \\ {}_{k+3/4}E^{z}_{l,m-1/4,n+1/2} \\ {}_{k+3/4}E^{z}_{l,m+1/4,n+1/2} \\ {}_{k+3/4}E^{x}_{l+1/2,m-1/4,n} \\ {}_{k+3/4}E^{x}_{l+1/2,m+1/4,n} \\ {}_{k+3/4}E^{x}_{l+1/2,m,n-1/4} \\ {}_{k+3/4}E^{x}_{l+1/2,m,n+1/4} \\ {}_{k+3/4}E^{y}_{l,m-1/2,n-1/4} \\ {}_{k+3/4}E^{y}_{l,m-1/2,n+1/4} \end{bmatrix} \cdot |k;\, l,\, m,\, n\rangle. \quad (61)$$

Analogously, $|F_{M1}\rangle$, defined by

$$|F_{M1}\rangle = Z \sum_{k,l,m,n=-\infty}^{+\infty} \begin{bmatrix} {}_{k+3/4}H^{z}_{l-1/4,m-1/2,n} \\ {}_{k+3/4}H^{z}_{l+1/4,m-1/2,n} \\ {}_{k+3/4}H^{y}_{l-1/4,m,n+1/2} \\ {}_{k+3/4}H^{y}_{l+1/4,m,n+1/2} \\ {}_{k+3/4}H^{x}_{l,m-1/4,n+1/2} \\ {}_{k+3/4}H^{x}_{l,m+1/4,n+1/2} \\ {}_{k+3/4}H^{z}_{l+1/2,m-1/4,n} \\ {}_{k+3/4}H^{z}_{l+1/2,m+1/4,n} \\ {}_{k+3/4}H^{y}_{l+1/2,m,n-1/4} \\ {}_{k+3/4}H^{y}_{l+1/2,m,n+1/4} \\ {}_{k+3/4}H^{x}_{l,m-1/2,n-1/4} \\ {}_{k+3/4}H^{x}_{l,m-1/2,n+1/4} \end{bmatrix} \cdot |k;\, l,\, m,\, n\rangle \quad (62)$$

summarizes all CBM values of the magnetic field components at the three shunt nodes of the expanded TLM nodes. In the same way, we define the electric field vector $|F_{E2}\rangle$ and the magnetic field vector $|F_{M2}\rangle$ combining all CBM values of the field components at the three series nodes of the expanded TLM nodes. The vector $|F_{E2}\rangle$ is given by

$$|F_{E2}\rangle = \sum_{k,l,m,n=-\infty}^{+\infty} \begin{bmatrix} {}_{k+1/4}E^{y}_{l+1/4,m-1/2,n} \\ {}_{k+1/4}E^{y}_{l+3/4,m-1/2,n} \\ {}_{k+1/4}E^{z}_{l+1/4,m,n+1/2} \\ {}_{k+1/4}E^{z}_{l+3/4,m,n+1/2} \\ {}_{k+1/4}E^{z}_{l,m-3/4,n+1/2} \\ {}_{k+1/4}E^{z}_{l,m-1/4,n+1/2} \\ {}_{k+1/4}E^{x}_{l+1/2,m-3/4,n} \\ {}_{k+1/4}E^{x}_{l+1/2,m-1/4,n} \\ {}_{k+1/4}E^{x}_{l+1/2,m,n+1/4} \\ {}_{k+1/4}E^{x}_{l+1/2,m,n+3/4} \\ {}_{k+1/4}E^{y}_{l,m-1/2,n+1/4} \\ {}_{k+1/4}E^{y}_{l,m-1/2,n+3/4} \end{bmatrix} \cdot |k;\, l,\, m,\, n\rangle \quad (63)$$

the vector $|F_{M2}\rangle$ by

$$|F_{M2}\rangle = Z \sum_{k,l,m,n=-\infty}^{+\infty} \begin{bmatrix} {}_{k+1/4}H^{z}_{l+1/4,m-1/2,n} \\ {}_{k+1/4}H^{z}_{l+3/4,m-1/2,n} \\ {}_{k+1/4}H^{y}_{l+1/4,m,n+1/2} \\ {}_{k+1/4}H^{y}_{l+3/4,m,n+1/2} \\ {}_{k+1/4}H^{x}_{l,m-3/4,n+1/2} \\ {}_{k+1/4}H^{x}_{l,m-1/4,n+1/2} \\ {}_{k+1/4}H^{z}_{l+1/2,m-3/4,n} \\ {}_{k+1/4}H^{z}_{l+1/2,m-1/4,n} \\ {}_{k+1/4}H^{y}_{l+1/2,m,n+1/4} \\ {}_{k+1/4}H^{y}_{l+1/2,m,n+3/4} \\ {}_{k+1/4}H^{x}_{l,m-1/2,n+1/4} \\ {}_{k+1/4}H^{x}_{l,m-1/2,n+3/4} \end{bmatrix} \cdot |k;\, l,\, m,\, n\rangle. \quad (64)$$

Rewriting (59) using the Hilbert space representation yields

$$\begin{aligned} &[0,\,0,\,1,\,1,\,1,\,1,\,0,\,0,\,0,\,0,\,0,\,0](1-\boldsymbol{T}_h)|F_{E1}\rangle \\ &\quad = [0,\,0,\,-1,\,1,\,1,\,-1,\,0,\,0,\,0,\,0,\,0,\,0] \\ &\qquad \cdot (1+\boldsymbol{T}_h)\eta_1|F_{M1}\rangle. \end{aligned} \quad (65)$$

We introduce wave amplitudes by relating them to the CBM values of the field components. The cell boundary mapping for the expanded TLM node is given by

$$\begin{aligned} |a_i\rangle &= 1/2(|F_{Ei}\rangle + P|F_{Mi}\rangle) \\ |b_i\rangle &= 1/2(|F_{Ei}\rangle - P|F_{Mi}\rangle) \end{aligned} \quad (66)$$

and

$$\begin{aligned} |F_{Ei}\rangle &= |a_i\rangle + |b_i\rangle \\ |F_{Mi}\rangle &= P(|a_i\rangle - |b_i\rangle) \end{aligned} \quad (67)$$

with $i = 1$ for the field components at the three series nodes of the expanded node and with $i = 2$ for the field components at the three shunt nodes of the expanded node. We have introduced the matrix

$$P = \begin{bmatrix} B & 0 & 0 \\ 0 & B & 0 \\ 0 & 0 & B \end{bmatrix} \quad (68)$$

with

$$B = \begin{bmatrix} 1 & 0 & 0 & 0 \\ 0 & -1 & 0 & 0 \\ 0 & 0 & -1 & 0 \\ 0 & 0 & 0 & 1 \end{bmatrix}. \quad (69)$$

The property $P^2 = 1$ ensures that the cell boundary mapping is a bijective one-to-one mapping between the forty-eight electric and magnetic field components and the forty-eight incident and scattered wave amplitudes at one expanded TLM node.

The vector of the incident wave amplitudes, $|a_i\rangle$, and the vector of the scattered wave amplitudes, $|b_i\rangle$, are defined by

$$|a_i\rangle = \sum_{k,l,m,n=-\infty}^{+\infty} {}_k\boldsymbol{a}_{i\,l,m,n}\,|k;\, l,\, m,\, n\rangle \quad (70)$$

and

$$|b_i\rangle = \sum_{k,l,m,n=-\infty}^{+\infty} {}_k\boldsymbol{b}_{i\,l,m,n}\,|k;\,l,\,m,\,n\rangle. \tag{71}$$

For $i = 1$, the vector $|a_1\rangle$ and the vector $|b_1\rangle$ summarize all incident and all scattered wave amplitudes at the three shunt nodes of the expanded TLM nodes. The vectors ${}_k\boldsymbol{a}_{1\,l,m,n}$ and ${}_k\boldsymbol{b}_{1\,l,m,n}$ are given by

$$\begin{aligned} {}_k\boldsymbol{a}_{1\,l,m,n} &= {}_k[a_1,\,a_2,\,a_5,\,a_6,\,a_{11},\,a_{12},\\ &\qquad a_{15},\,a_{16},\,a_{17},\,a_{18},\,a_{21},\,a_{22}]^T_{l,m,n}\\ {}_k\boldsymbol{b}_{1\,l,m,n} &= {}_k[b_1,\,b_2,\,b_5,\,b_6,\,b_{11},\,b_{12},\\ &\qquad b_{15},\,b_{16},\,b_{17},\,b_{18},\,b_{21},\,b_{22}]^T_{l,m,n}. \end{aligned} \tag{72}$$

For $i = 2$, the vector $|a_2\rangle$ and the vector $|b_2\rangle$ summarize all incident and all scattered wave amplitudes at the three series nodes of the expanded TLM nodes. The vectors ${}_k\boldsymbol{a}_{2\,l,m,n}$ and ${}_k\boldsymbol{b}_{2\,l,m,n}$ are given by

$$\begin{aligned} {}_k\boldsymbol{a}_{2\,l,m,n} &= {}_k[a_3,\,a_4,\,a_7,\,a_8,\,a_9,\,a_{10},\\ &\qquad a_{13},\,a_{14},\,a_{19},\,a_{20},\,a_{23},\,a_{24}]^T_{l,m,n}\\ {}_k\boldsymbol{b}_{2\,l,m,n} &= {}_k[b_3,\,b_4,\,b_7,\,b_8,\,b_9,\,b_{10},\\ &\qquad b_{13},\,b_{14},\,b_{19},\,b_{20},\,b_{23},\,b_{24}]^T_{l,m,n}. \end{aligned} \tag{73}$$

For each boundary surface, the wave amplitudes incident into one two-dimensional TLM node are identical with the wave amplitudes scattered from the neighboring two-dimensional TLM nodes. This relation is expressed by

$$|a_1\rangle = \boldsymbol{\Gamma}_1\,|b_2\rangle$$

and

$$|a_2\rangle = \boldsymbol{\Gamma}_2\,|b_1\rangle, \tag{74}$$

where the connection operators $\boldsymbol{\Gamma}_i$ are given by

$$\begin{aligned} \boldsymbol{\Gamma}_1 = {} & \boldsymbol{X}(\boldsymbol{\Delta}_{1,2} + \boldsymbol{\Delta}_{3,4}) + \boldsymbol{\Delta}_{2,1} + \boldsymbol{\Delta}_{4,3} + \boldsymbol{\Delta}_{5,6} + \boldsymbol{\Delta}_{7,8}\\ & + \boldsymbol{Y}^\dagger(\boldsymbol{\Delta}_{6,5} + \boldsymbol{\Delta}_{8,7}) + \boldsymbol{Z}(\boldsymbol{\Delta}_{9,10} + \boldsymbol{\Delta}_{11,12})\\ & + \boldsymbol{\Delta}_{10,9} + \boldsymbol{\Delta}_{12,11} \end{aligned} \tag{75}$$

and

$$\boldsymbol{\Gamma}_2 = \boldsymbol{\Gamma}_1^\dagger \tag{76}$$

with the 12×12 (m, n)-matrix $(\boldsymbol{\Delta}_{i,j})_{m,n} = \delta_{i,m}\,\delta_{j,n}$ and with the shift operators $\boldsymbol{X}$ and its Hermitian conjugate $\boldsymbol{X}^\dagger$ defined by

$$\begin{aligned} \boldsymbol{X}\,|k;\,l,\,m,\,n\rangle &= |k;\,l+1,\,m,\,n\rangle\\ \boldsymbol{X}^\dagger\,|k;\,l,\,m,\,n\rangle &= |k;\,l-1,\,m,\,n\rangle. \end{aligned} \tag{77}$$

The operators $\boldsymbol{Y}$, $\boldsymbol{Z}$, $\boldsymbol{Y}^\dagger$, and $\boldsymbol{Z}^\dagger$ are defined in a similar way for the discrete coordinates m and n.

We apply the cell boundary mapping to obtain the discretized field equations for wave amplitudes. Choosing $\eta_1 = 1$ yields one discretized field equations for wave amplitudes

$$\begin{aligned} &[0,\,0,\,1,\,1,\,1,\,1,\,0,\,0,\,0,\,0,\,0,\,0]\,|b_1\rangle\\ &\quad = [0,\,0,\,1,\,1,\,1,\,1,\,0,\,0,\,0,\,0,\,0,\,0]\boldsymbol{T}_h\,|a_1\rangle. \end{aligned} \tag{78}$$

To determine the 4×4-scattering matrix of one two-dimensional shunt node, we need four discretized field equations for wave amplitudes. Thus, in total, we need twenty-four discretized field equations for wave amplitudes to determine the two 12×12-scattering matrices of the expanded TLM node.

In the following, we derive the additional three discretized field equations for wave amplitudes to determine the scattering matrix of one two-dimensional shunt node. Sampling (6) and (7) in the cell boundaries and introducing the CBM values of the field components, we obtain

$$\begin{aligned} &\begin{bmatrix} 0 & 0 & -1 & 1 & 0 & 0 & 0 & 0 & 0 & 0 & 0 & 0\\ 0 & 0 & 0 & 0 & 1 & -1 & 0 & 0 & 0 & 0 & 0 & 0\\ 0 & 0 & 1 & 1 & -1 & -1 & 0 & 0 & 0 & 0 & 0 & 0 \end{bmatrix}\\ &\quad \cdot (1 + \boldsymbol{T}_h)\eta_2\,|F_{E1}\rangle =\\ &\quad \begin{bmatrix} 0 & 0 & 1 & 1 & 0 & 0 & 0 & 0 & 0 & 0 & 0 & 0\\ 0 & 0 & 0 & 0 & 1 & 1 & 0 & 0 & 0 & 0 & 0 & 0\\ 0 & 0 & -1 & 1 & -1 & 1 & 0 & 0 & 0 & 0 & 0 & 0 \end{bmatrix}\\ &\quad \cdot (1 - \boldsymbol{T}_h)\,|F_{M1}\rangle. \end{aligned} \tag{79}$$

For the derivation of (79), we have also used the relations

$$\begin{aligned} &\begin{bmatrix} 0 & 0 & 1 & -1 & 0 & 0 & 0 & 0 & 1 & -1 & 0 & 0\\ 0 & 0 & 0 & 0 & 1 & -1 & 0 & 0 & 0 & 0 & 1 & -1 \end{bmatrix}\\ &\quad \cdot (\boldsymbol{T}_h^\dagger + 1)\,|F_{E2}\rangle = 0. \end{aligned} \tag{80}$$

These relations are necessary to derive all of the four discretized field equations for wave amplitudes at one two-dimensional shunt node. In total, for the derivation of the complete TLM scheme for the expanded node, we need six of these relations given by (80)

$$\begin{aligned} &[1 \quad -1 \quad 0 \quad 0 \quad 0 \quad 0 \quad 1 \quad -1 \quad 0 \quad 0 \quad 0 \quad 0]\\ &\quad \cdot (\boldsymbol{T}_h^\dagger + 1)\,|F_{E2}\rangle = 0 \end{aligned} \tag{81}$$

and

$$\begin{aligned} &\begin{bmatrix} 0 & 0 & 1 & -1 & 1 & -1 & 0 & 0 & 0 & 0 & 0 & 0\\ 1 & -1 & 0 & 0 & 0 & 0 & 0 & 0 & 0 & 0 & 1 & -1\\ 0 & 0 & 0 & 0 & 0 & 0 & 1 & -1 & 1 & -1 & 0 & 0 \end{bmatrix}\\ &\quad \cdot (\boldsymbol{T}_h^\dagger + 1)\,|F_{M1}\rangle = 0. \end{aligned} \tag{82}$$

The six relations for the CBM values of the electric and magnetic field components are not derived from Maxwell's equations. These relations are imposed arbitrarily causing the scattering at the three shunt nodes to be shifted by half a discretization interval in space and time with respect to the scattering at the three series nodes.

We introduce wave amplitudes by the cell boundary mapping for the expanded TLM node. Choosing $\eta_2 = \eta_1 = 1$ yields

$$Z_0 = Z \quad \text{and} \quad \frac{c}{c_m} = \frac{1}{2} \tag{83}$$

where we have introduced the mesh pulse velocity $c_m = \Delta l/\Delta t$. These results are well-known from literature [2]. From (79), we obtain

$$\begin{aligned} &\begin{bmatrix} 0 & 0 & -1 & 1 & 0 & 0 & 0 & 0 & 0 & 0 & 0 & 0\\ 0 & 0 & 0 & 0 & 1 & -1 & 0 & 0 & 0 & 0 & 0 & 0\\ 0 & 0 & 1 & 1 & -1 & -1 & 0 & 0 & 0 & 0 & 0 & 0 \end{bmatrix} |b_1\rangle =\\ &\begin{bmatrix} 0 & 0 & 1 & -1 & 0 & 0 & 0 & 0 & 0 & 0 & 0 & 0\\ 0 & 0 & 0 & 0 & -1 & 1 & 0 & 0 & 0 & 0 & 0 & 0\\ 0 & 0 & -1 & -1 & 1 & 1 & 0 & 0 & 0 & 0 & 0 & 0 \end{bmatrix} \boldsymbol{T}_h\,|a_1\rangle. \end{aligned} \tag{84}$$

Equations (78) and (84) determine the 4×4-scattering matrix of one two-dimensional shunt node of the expanded TLM node uniquely. Deriving the remaining five 4×4-scattering matrices of the expanded node in the same way, we obtain

$$|b_i\rangle = \boldsymbol{T}_h \boldsymbol{S}_i |a_i\rangle \tag{85}$$

with the two 12×12-scattering matrices of the expanded node

$$\boldsymbol{S}_i = \begin{bmatrix} \boldsymbol{S}_{i1} & \boldsymbol{S}_{i2} & \boldsymbol{S}_{i2}^T \\ \boldsymbol{S}_{i2}^T & \boldsymbol{S}_{i1} & \boldsymbol{S}_{i2} \\ \boldsymbol{S}_{i2} & \boldsymbol{S}_{i2}^T & \boldsymbol{S}_{i1} \end{bmatrix} \tag{86}$$

where we have introduced

$$\boldsymbol{S}_{11} = \tfrac{1}{2} \begin{bmatrix} -1 & 1 & 0 & 0 \\ 1 & -1 & 0 & 0 \\ 0 & 0 & -1 & 1 \\ 0 & 0 & 1 & -1 \end{bmatrix}$$

and

$$\boldsymbol{S}_{12} = \tfrac{1}{2} \begin{bmatrix} 0 & 0 & 0 & 0 \\ 0 & 0 & 0 & 0 \\ 1 & 1 & 0 & 0 \\ 1 & 1 & 0 & 0 \end{bmatrix} \tag{87}$$

as well as

$$\boldsymbol{S}_{22} = \begin{bmatrix} 1 & 1 & 0 & 0 \\ 1 & 1 & 0 & 0 \\ 0 & 0 & 1 & 1 \\ 0 & 0 & 1 & 1 \end{bmatrix}$$

and

$$\boldsymbol{S}_{21} = \begin{bmatrix} 0 & 0 & 1 & -1 \\ 0 & 0 & -1 & 1 \\ 0 & 0 & 0 & 0 \\ 0 & 0 & 0 & 0 \end{bmatrix}. \tag{88}$$

B. Dispersion Analysis

We eliminate the vectors of the scattered wave amplitudes and the vector $|a_2\rangle$. Using (74) and (85), we obtain

$$(\boldsymbol{T} \quad \boldsymbol{\Gamma}_1 \quad \boldsymbol{S}_2 \quad \boldsymbol{\Gamma}_2 \quad \boldsymbol{S}_1 - 1)\,|a_1\rangle = 0 \tag{89}$$

where we have introduced the time shift operator

$$\boldsymbol{T}|k;\, l,\, m,\, n\rangle = |k+1;\, l,\, m,\, n\rangle. \tag{90}$$

As shown in [10], [14], (89) in frequency domain is given by the eigenvalue equation

$$(\boldsymbol{\Gamma}_1 \quad \boldsymbol{S}_2 \quad \boldsymbol{\Gamma}_2 \quad \boldsymbol{S}_1 - e^{\jmath\Omega} \quad 1)\,|a_1(\Omega)\rangle_m = 0. \tag{91}$$

As shown for the FDTD method, the vector $|a(\Omega)\rangle_m$ is given by

$$|a(\Omega)\rangle_m =_t \langle \Omega \,|\, a\rangle = \vec{a}_1(\chi,\, \eta,\, \xi) e^{-\jmath k\Omega} |\chi,\, \eta,\, \xi\rangle \tag{92}$$

with the vector of the plane wave amplitudes

$$\vec{a}_1(\chi,\, \eta,\, \xi) = \sum_{l,\, m,\, n=-\infty}^{+\infty} {}_k\boldsymbol{a}_{1\, l,\, m,\, n} e^{-\jmath(\chi l + \eta m + \xi n)} \tag{93}$$

if we restrict our investigations to electromagnetic fields composed of plane waves. In this case, the calculation of the inner product of $\langle \chi,\, \eta,\, \xi|$ and (91) yields the representation of (91) in wave vector domain

$$(\overline{\boldsymbol{\Gamma}}_1 \quad \boldsymbol{S}_2 \quad \overline{\boldsymbol{\Gamma}}_2 \quad \boldsymbol{S}_1 - e^{\jmath\Omega})\vec{a}_1(\chi,\, \eta,\, \xi) = 0 \tag{94}$$

where we have introduced the connection operators in wave vector domain

$$\begin{aligned} \overline{\boldsymbol{\Gamma}}_1 = {} & e^{-\jmath\chi}(\boldsymbol{\Delta}_{1,2} + \boldsymbol{\Delta}_{3,4}) + \boldsymbol{\Delta}_{2,1} + \boldsymbol{\Delta}_{4,3} + \boldsymbol{\Delta}_{5,6} + \boldsymbol{\Delta}_{7,8} \\ & + e^{\jmath\eta}(\boldsymbol{\Delta}_{6,5} + \boldsymbol{\Delta}_{8,7}) + e^{-\jmath\xi}(\boldsymbol{\Delta}_{9,10} + \boldsymbol{\Delta}_{11,12}) \\ & + \boldsymbol{\Delta}_{10,9} + \boldsymbol{\Delta}_{12,11} \end{aligned} \tag{95}$$

and

$$\overline{\boldsymbol{\Gamma}}_2 = \overline{\boldsymbol{\Gamma}}_1^{\dagger}. \tag{96}$$

Equation (94) has nontrivial solutions if

$$\det\left(\overline{\boldsymbol{\Gamma}}_1 \quad \boldsymbol{S}_2 \quad \overline{\boldsymbol{\Gamma}}_2 \quad \boldsymbol{S}_1 - e^{\jmath\Omega}\right) = 0. \tag{97}$$

From (97), we calculate the eigenvalues $\lambda_i = e^{\jmath\Omega_i}$ as

$$\begin{aligned} \lambda_{1,2} &= C_2 + \sqrt{(C_2)^2 - 1} \\ \lambda_{3,4} &= C_2 - \sqrt{(C_2)^2 - 1} \\ \lambda_{5,6} &= 1 \\ \lambda_{7,\cdots,12} &= -1 \end{aligned} \tag{98}$$

with

$$C_2 = \tfrac{1}{2}[\cos(\chi) + \cos(\eta) + \cos(\xi) + 1]. \tag{99}$$

The eigenvalues $\lambda_1, \cdots, \lambda_6$ are identical with the eigenvalues λ_i of Yee's FDTD scheme for the stability factor $s = 1/2$. The eigenvectors corresponding to these eigenvalues describe solutions of the TLM scheme which converge to solutions of Maxwell's equations for frequencies approaching zero. We call these eigenvectors the physical eigenvectors of the TLM method. The eigenvalues $\lambda_7, \cdots, \lambda_{12}$ have eigenvectors describing solutions of the TLM scheme which do not converge to solutions of Maxwell's equations for frequencies approaching zero. $\lambda = -1$ implies $\Omega = \pi$, thus the eigenvalues $\lambda_7, \cdots, \lambda_{12}$ have unphysical eigenvectors describing stationary solutions in the TLM mesh oscillating with the frequency $1/(2\Delta t)$. In a mesh with expanded TLM nodes, there are physical eigenvectors with the same dispersion characteristics as the FDTD eigenvectors and unphysical eigenvectors which do not exist in the FDTD mesh.

IV. The TLM Method with Asymmetrical Condensed Node

The asymmetrical condensed TLM node depicted in Fig. 2 is composed of three two-dimensional TLM shunt nodes and three two-dimensional TLM series nodes. In contrast to the expanded node, the six two-dimensional nodes are condensed in the center of the three-dimensional cubic TLM cell leading to a 12×12-scattering matrix [2], [8]. For the derivation of the three-dimensional TLM method with asymmetrical condensed node, we use rectangular pulse functions as subdomain basis functions with respect to space and time. In contrast to the derivation of the FDTD method and the TLM method with expanded node, the field expansions of the magnetic field

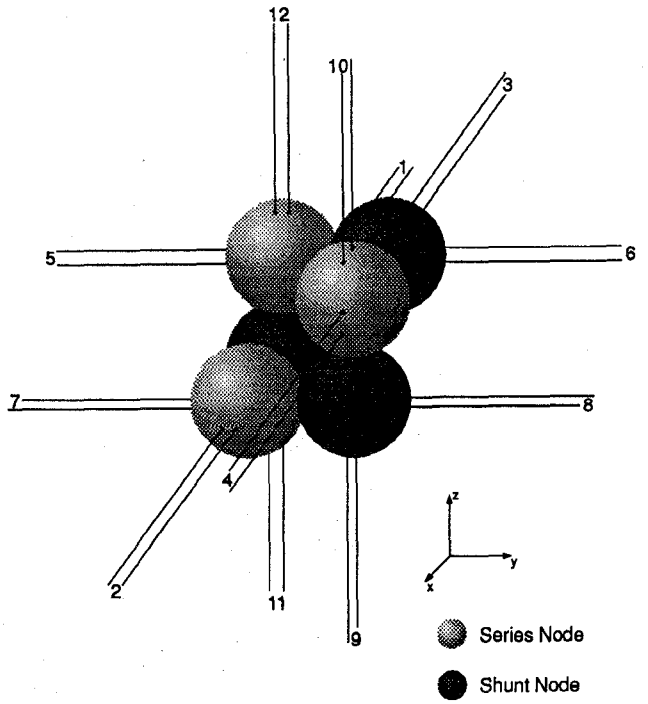

Fig. 2. The three-dimensional asymmetrical condensed TLM node.

components are identical with the field expansions of the electric field components. The six linearly independent field components are defined at the center of the TLM cell. As test functions, according to Galerkin's method [4], we use pulse functions in space and time, too. The derivation of the asymmetrical condensed TLM node is similar to the derivation of the two-dimensional TLM method [5].

A. Field Theoretic Derivation

We expand the field components in

$$\begin{aligned}
E_x(\vec{x}, t) &= \sum_{k,l,m,n=-\infty}^{+\infty} {}_kE^x_{l,m,n} h_k(t) h_l(x) K_{m,n}(y, z) \\
E_y(\vec{x}, t) &= \sum_{k,l,m,n=-\infty}^{+\infty} {}_kE^y_{l,m,n} h_k(t) h_m(y) K_{l,n}(x, z) \\
E_z(\vec{x}, t) &= \sum_{k,l,m,n=-\infty}^{+\infty} {}_kE^z_{l,m,n} h_k(t) h_n(z) K_{l,m}(x, y) \\
H_x(\vec{x}, t) &= \sum_{k,l,m,n=-\infty}^{+\infty} {}_kH^x_{l,m,n} h_k(t) h_l(x) K_{m,n}(y, z) \\
H_y(\vec{x}, t) &= \sum_{k,l,m,n=-\infty}^{+\infty} {}_kH^y_{l,m,n} h_k(t) h_m(y) K_{l,n}(x, z) \\
H_z(\vec{x}, t) &= \sum_{k,l,m,n=-\infty}^{+\infty} {}_kH^z_{l,m,n} h_k(t) h_n(z) K_{l,m}(x, y).
\end{aligned} \tag{100}$$

The functions $K_{l,m}(x, y)$ are given by the product of two rectangular pulse functions as

$$K_{l,m}(x, y) = h_l(x) h_m(y). \tag{101}$$

We insert the field expansions in (3)–(8) and sample the field components with respect to space using the functions

$$\begin{aligned}
L^1_{l,m}(x, y) = h&\left(\frac{x}{2\Delta x} + \frac{y}{2\Delta y} - \frac{l+m}{2}\right) \\
&\cdot h\left(\frac{x}{2\Delta x} - \frac{y}{2\Delta y} - \frac{l-m}{2}\right).
\end{aligned} \tag{102}$$

The functions $L^1_{l,m}(x, y)$ are squares in the x–y plane rotated by 45° around the z-axis with respect to the functions $K_{l,m}(x, y)$. For the spatial sampling, we need

$$\begin{aligned}
&\int_{-\infty}^{+\infty}\int_{-\infty}^{+\infty} L^1_{l,m}(x, y) K_{l',m'}(x, y)\, dx\, dy \\
&\quad = \frac{\Delta x\, \Delta y}{4} (\delta_{l,l'\pm1}\delta_{m,m'} \\
&\qquad + \delta_{l,l'}\delta_{m,m'\pm1} + 4\,\delta_{l,l'}\delta_{m,m'})
\end{aligned} \tag{103}$$

$$\begin{aligned}
&\int_{-\infty}^{+\infty}\int_{-\infty}^{+\infty} L^1_{l,m}(x, y) \frac{\partial K_{l',m'}(x,y)}{\partial x}\, dx\, dy \\
&\quad = \delta_{l,l'+1}\delta_{m,m'} - \delta_{l,l'-1}\delta_{m,m'}
\end{aligned} \tag{104}$$

and

$$\begin{aligned}
&\int_{-\infty}^{+\infty}\int_{-\infty}^{+\infty} L^1_{l,m}(x, y) \frac{\partial K_{l',m'}(x,y)}{\partial y}\, dx\, dy \\
&\quad = \delta_{l,l'}\delta_{m,m'+1} - \delta_{l,l'}\delta_{m,m'-1}.
\end{aligned} \tag{105}$$

Furthermore, we need

$$\begin{aligned}
&\int_{-\infty}^{+\infty} h_m(x) h_{m'\pm1/2}(x)\, dx \\
&\quad = \frac{\Delta x}{2} (\delta_{m,m'} + \delta_{m,m'+1})
\end{aligned} \tag{106}$$

for sampling the field expansions with respect to time. Sampling (3) with $h_{k+1/2}(t) h_l(x) L^1_{m,n}(y, z)$, we obtain

$$\begin{aligned}
&4\,{}_{k+1}E^x_{l,m,n} + {}_{k+1}E^x_{l,m+1,n} + {}_{k+1}E^x_{l,m-1,n} \\
&\quad + {}_{k+1}E^x_{l,m,n+1} + {}_{k+1}E^x_{l,m,n-1} - 4\,{}_kE^x_{l,m,n} \\
&\quad - {}_kE^x_{l,m+1,n} - {}_kE^x_{l,m-1,n} - {}_kE^x_{l,m,n+1} - {}_kE^x_{l,m,n-1} \\
&\quad = \eta_1({}_{k+1}H^z_{l,m+1,n} + {}_kH^z_{l,m+1,n} \\
&\qquad - {}_{k+1}H^z_{l,m-1,n} - {}_kH^z_{l,m-1,n}) \\
&\qquad - \eta_1({}_{k+1}H^y_{l,m,n+1} + {}_kH^y_{l,m,n+1} \\
&\qquad - {}_{k+1}H^y_{l,m,n-1} - {}_kH^y_{l,m,n-1})
\end{aligned} \tag{107}$$

where we have chosen Δl according to (19). We define the field vector

$$\begin{aligned}
|F'\rangle = \sum_{k,l,m,n=-\infty}^{+\infty} {}_k[&E_x, E_y, E_z, ZH_x, \\
&ZH_y, ZH_z]^T_{l,m,n} |k; l, m, n\rangle
\end{aligned} \tag{108}$$

as a vector in $\mathcal{H}_F$. Sampling (4)–(8) in the same way, we obtain the six discretized field equations

$$\boldsymbol{M}_1 |F'\rangle = 0 \tag{109}$$

with (110), shown at the bottom of the next page, where we have used the abbreviations

$$\begin{aligned}
\boldsymbol{D}_{tx} &= (1 + \boldsymbol{T})^{-1}(1 - \boldsymbol{T})(4 + \boldsymbol{Y} + \boldsymbol{Z} + \boldsymbol{Y}^\dagger + \boldsymbol{Z}^\dagger) \\
\boldsymbol{D}_{ty} &= (1 + \boldsymbol{T})^{-1}(1 - \boldsymbol{T})(4 + \boldsymbol{X} + \boldsymbol{Z} + \boldsymbol{X}^\dagger + \boldsymbol{Z}^\dagger) \\
\boldsymbol{D}_{tz} &= (1 + \boldsymbol{T})^{-1}(1 - \boldsymbol{T})(4 + \boldsymbol{X} + \boldsymbol{Y} + \boldsymbol{X}^\dagger + \boldsymbol{Y}^\dagger).
\end{aligned} \tag{111}$$

In the same way as for the expanded TLM node, we introduce the CBM values of the field components as the values of the series expansions for the field components at the cell boundaries. For TLM with asymmetrical condensed node, the value of the series expansion is identical with the mean value of the field components of two neighboring cells. For example, the CBM value $E^x_{l,\,m+1/2,\,n}$ is given by

$$ {}_kE^x_{l,\,m+1/2,\,n} = \tfrac{1}{2}({}_kE^x_{l,\,m+1,\,n} + {}_kE^x_{l,\,m,\,n}). \tag{112} $$

We define the electric field vector $|F_E\rangle$ and the magnetic field vector $|F_M\rangle$ as vectors in the Hilbert space $\mathcal{H}_W$. The electric field vector

$$ |F_E\rangle = \sum_{k,\,l,\,m,\,n=-\infty}^{+\infty} \begin{bmatrix} {}_k[E_y]_{l-1/2,\,m,\,n} \\ {}_k[E_y]_{l+1/2,\,m,\,n} \\ {}_k[E_z]_{l-1/2,\,m,\,n} \\ {}_k[E_z]_{l+1/2,\,m,\,n} \\ {}_k[E_z]_{l,\,m-1/2,\,n} \\ {}_k[E_z]_{l,\,m+1/2,\,n} \\ {}_k[E_x]_{l,\,m-1/2,\,n} \\ {}_k[E_x]_{l,\,m+1/2,\,n} \\ {}_k[E_x]_{l,\,m,\,n-1/2} \\ {}_k[E_x]_{l,\,m,\,n+1/2} \\ {}_k[E_y]_{l,\,m,\,n-1/2} \\ {}_k[E_y]_{l,\,m,\,n+1/2} \end{bmatrix} \cdot |k;\, l,\, m,\, n\rangle \tag{113} $$

combines all electric field components in the cell boundary surfaces of the TLM mesh with asymmetrical condensed nodes at all discrete time points $k\Delta t$. The magnetic field vector

$$ |F_M\rangle = Z \sum_{k,\,l,\,m,\,n=-\infty}^{+\infty} \begin{bmatrix} {}_k[H_z]_{l-1/2,\,m,\,n} \\ {}_k[H_z]_{l+1/2,\,m,\,n} \\ {}_k[H_y]_{l-1/2,\,m,\,n} \\ {}_k[H_y]_{l+1/2,\,m,\,n} \\ {}_k[H_x]_{l,\,m-1/2,\,n} \\ {}_k[H_x]_{l,\,m+1/2,\,n} \\ {}_k[H_z]_{l,\,m-1/2,\,n} \\ {}_k[H_z]_{l,\,m+1/2,\,n} \\ {}_k[H_y]_{l,\,m,\,n-1/2} \\ {}_k[H_y]_{l,\,m,\,n+1/2} \\ {}_k[H_x]_{l,\,m,\,n-1/2} \\ {}_k[H_x]_{l,\,m,\,n+1/2} \end{bmatrix} \cdot |k;\, l,\, m,\, n\rangle \tag{114} $$

summarizes all magnetic field components in the cell boundary surfaces of the TLM mesh with asymmetrical condensed nodes. The relationship between the field components at the center of a TLM cell and the CBM values of the field components is given by

$$ |F_E\rangle = \tfrac{1}{2} \begin{bmatrix} 0 & 1+\boldsymbol{X} & 0 & 0 & 0 & 0 \\ 0 & 1+\boldsymbol{X}^\dagger & 0 & 0 & 0 & 0 \\ 0 & 0 & 1+\boldsymbol{X} & 0 & 0 & 0 \\ 0 & 0 & 1+\boldsymbol{X}^\dagger & 0 & 0 & 0 \\ 0 & 0 & 1+\boldsymbol{Y} & 0 & 0 & 0 \\ 0 & 0 & 1+\boldsymbol{Y}^\dagger & 0 & 0 & 0 \\ 1+\boldsymbol{Y} & 0 & 0 & 0 & 0 & 0 \\ 1+\boldsymbol{Y}^\dagger & 0 & 0 & 0 & 0 & 0 \\ 1+\boldsymbol{Z} & 0 & 0 & 0 & 0 & 0 \\ 1+\boldsymbol{Z}^\dagger & 0 & 0 & 0 & 0 & 0 \\ 0 & 1+\boldsymbol{Z} & 0 & 0 & 0 & 0 \\ 0 & 1+\boldsymbol{Z}^\dagger & 0 & 0 & 0 & 0 \end{bmatrix} |F'\rangle \tag{115} $$

and

$$ |F_M\rangle = \tfrac{1}{2} \begin{bmatrix} 0 & 0 & 0 & 0 & 0 & 1+\boldsymbol{X} \\ 0 & 0 & 0 & 0 & 0 & 1+\boldsymbol{X}^\dagger \\ 0 & 0 & 0 & 0 & 1+\boldsymbol{X} & 0 \\ 0 & 0 & 0 & 0 & 1+\boldsymbol{X}^\dagger & 0 \\ 0 & 0 & 0 & 1+\boldsymbol{Y} & 0 & 0 \\ 0 & 0 & 0 & 1+\boldsymbol{Y}^\dagger & 0 & 0 \\ 0 & 0 & 0 & 0 & 0 & 1+\boldsymbol{Y} \\ 0 & 0 & 0 & 0 & 0 & 1+\boldsymbol{Y}^\dagger \\ 0 & 0 & 0 & 0 & 1+\boldsymbol{Z} & 0 \\ 0 & 0 & 0 & 0 & 1+\boldsymbol{Z}^\dagger & 0 \\ 0 & 0 & 0 & 1+\boldsymbol{Z} & 0 & 0 \\ 0 & 0 & 0 & 1+\boldsymbol{Z}^\dagger & 0 & 0 \end{bmatrix} |F'\rangle. \tag{116} $$

$$ \boldsymbol{M}_1 = \begin{bmatrix} \frac{1}{\eta_1}\boldsymbol{D}_{tx} & 0 & 0 & 0 & \boldsymbol{Z}^\dagger - \boldsymbol{Z} & \boldsymbol{Y} - \boldsymbol{Y}^\dagger \\ 0 & \frac{1}{\eta_1}\boldsymbol{D}_{ty} & 0 & \boldsymbol{Z} - \boldsymbol{Z}^\dagger & 0 & \boldsymbol{X}^\dagger - \boldsymbol{X} \\ 0 & 0 & \frac{1}{\eta_1}\boldsymbol{D}_{tz} & \boldsymbol{Y}^\dagger - \boldsymbol{Y} & \boldsymbol{X} - \boldsymbol{X}^\dagger & 0 \\ 0 & \boldsymbol{Z} - \boldsymbol{Z}^\dagger & \boldsymbol{Y}^\dagger - \boldsymbol{Y} & \frac{1}{\eta_2}\boldsymbol{D}_{tx} & 0 & 0 \\ \boldsymbol{Z}^\dagger - \boldsymbol{Z} & 0 & \boldsymbol{X} - \boldsymbol{X}^\dagger & 0 & \frac{1}{\eta_2}\boldsymbol{D}_{ty} & 0 \\ \boldsymbol{Y} - \boldsymbol{Y}^\dagger & \boldsymbol{X}^\dagger - \boldsymbol{X} & 0 & 0 & 0 & \frac{1}{\eta_2}\boldsymbol{D}_{tz} \end{bmatrix} \tag{110} $$

We use the symmetrical representation of the scattering matrix as introduced for the symmetrical condensed node [7], [18]. Then, the cell boundary mapping for the asymmetrical condensed node is identical with the cell boundary mapping for the symmetrical condensed node given by

$$|a\rangle = 1/2(|F_E\rangle + P|F_M\rangle)$$
$$|b\rangle = 1/2(|F_E\rangle - P|F_M\rangle) \tag{117}$$

and

$$|F_E\rangle = |a\rangle + |b\rangle$$
$$|F_M\rangle = P(|a\rangle - |b\rangle) \tag{118}$$

with the matrix P according to (68) and (69). The property $P^2 = 1$ ensures that the cell boundary mapping is a bijective one-to-one mapping between the twenty-four electric and magnetic field components and the twenty-four incident and scattered wave amplitudes at one asymmetrical condensed TLM node.

The vector of the incident wave amplitudes, $|a\rangle$, and the vector of the scattered wave amplitudes, $|b\rangle$, are defined by

$$|a\rangle = \sum_{k,l,m,n=-\infty}^{+\infty} {}_k\boldsymbol{a}_{l,m,n}\,|k;\, l,\, m,\, n\rangle \tag{119}$$

and

$$|b\rangle = \sum_{k,l,m,n=-\infty}^{+\infty} {}_k\boldsymbol{b}_{l,m,n}\,|k;\, l,\, m,\, n\rangle \tag{120}$$

with

$$\begin{aligned} {}_k\boldsymbol{a}_{l,m,n} &= {}_k[a_1,\, a_2,\, a_3,\, a_4,\, a_5,\, a_6,\\ &\qquad a_7,\, a_8,\, a_9,\, a_{10},\, a_{11},\, a_{12}]^T_{l,m,n}\\ {}_k\boldsymbol{b}_{l,m,n} &= {}_k[b_1,\, b_2,\, b_3,\, b_4,\, b_5,\, b_6,\\ &\qquad b_7,\, b_8,\, b_9,\, b_{10},\, b_{11},\, b_{12}]^T_{l,m,n}. \end{aligned} \tag{121}$$

Since the CBM values of the field components are also specified in the neighboring cell boundary surfaces, twelve CBM values for each TLM cell are linearly independent. Specifying e.g., all twelve incident wave amplitudes per TLM cell yields a complete description of the field state. For each boundary surface, the wave amplitudes incident into one three-dimensional TLM cell are identical with the wave amplitudes scattered from the neighboring TLM cells. This relation is expressed by

$$|a\rangle = \boldsymbol{\Gamma}\,|b\rangle$$

and

$$|b\rangle = \boldsymbol{\Gamma}\,|a\rangle. \tag{122}$$

The connection operator

$$\begin{aligned} \boldsymbol{\Gamma} &= \boldsymbol{X}(\boldsymbol{\Delta}_{1,2} + \boldsymbol{\Delta}_{3,4}) + \boldsymbol{X}^{\dagger}(\boldsymbol{\Delta}_{2,1} + \boldsymbol{\Delta}_{4,3})\\ &\quad + \boldsymbol{Y}(\boldsymbol{\Delta}_{5,6} + \boldsymbol{\Delta}_{7,8}) + \boldsymbol{Y}^{\dagger}(\boldsymbol{\Delta}_{6,5} + \boldsymbol{\Delta}_{8,7})\\ &\quad + \boldsymbol{Z}(\boldsymbol{\Delta}_{9,10} + \boldsymbol{\Delta}_{11,12}) + \boldsymbol{Z}^{\dagger}(\boldsymbol{\Delta}_{10,9} + \boldsymbol{\Delta}_{12,11}) \end{aligned} \tag{123}$$

is identical with the connection operator of the symmetrical condensed TLM node [7].

We rewrite (109) in terms of the CBM values of the field components and apply the cell boundary mapping for the asymmetrical condensed TLM node. Choosing $\eta_1 = \eta_2 = 1$ yielding again (83), we obtain six discretized field equations for wave amplitudes

$$\begin{bmatrix} 0 & 0 & 0 & 0 & 0 & 0 & 1 & 1 & 1 & 1 & 0 & 0\\ 1 & 1 & 0 & 0 & 0 & 0 & 0 & 0 & 0 & 0 & 1 & 1\\ 0 & 0 & 1 & 1 & 1 & 1 & 0 & 0 & 0 & 0 & 0 & 0\\ 0 & 0 & 0 & 0 & -1 & 1 & 0 & 0 & 0 & 0 & 1 & -1\\ 0 & 0 & 1 & -1 & 0 & 0 & 0 & 0 & -1 & 1 & 0 & 0\\ -1 & 1 & 0 & 0 & 0 & 0 & 1 & -1 & 0 & 0 & 0 & 0 \end{bmatrix} |b\rangle =$$
$$\begin{bmatrix} 0 & 0 & 0 & 0 & 0 & 0 & 1 & 1 & 1 & 1 & 0 & 0\\ 1 & 1 & 0 & 0 & 0 & 0 & 0 & 0 & 0 & 0 & 1 & 1\\ 0 & 0 & 1 & 1 & 1 & 1 & 0 & 0 & 0 & 0 & 0 & 0\\ 0 & 0 & 0 & 0 & 1 & -1 & 0 & 0 & 0 & 0 & -1 & 1\\ 0 & 0 & -1 & 1 & 0 & 0 & 0 & 0 & 1 & -1 & 0 & 0\\ 1 & -1 & 0 & 0 & 0 & 0 & -1 & 1 & 0 & 0 & 0 & 0 \end{bmatrix} \boldsymbol{T}\,|a\rangle. \tag{124}$$

Note that these six discretized field equations for wave amplitudes are identical with six discretized field equations for wave amplitudes used in the derivation of the symmetrical condensed node [7].

The scattering of the wave amplitudes at one asymmetrical condensed node is described by a 12×12-scattering matrix. Thus, we need another six discretized field equations for wave amplitudes to determine the scattering matrix uniquely. We obtain these additional discretized field equations by sampling the electromagnetic field asymmetrically with respect to space using the test functions

$$\begin{aligned} L^2_{m,n}(x, y) &= h\left(\frac{x}{\Delta x} + \frac{y}{\Delta y} - m - n\right)\\ &\quad \cdot h\left(\frac{x}{\Delta x} - \frac{y}{\Delta y} - m + n\right) \end{aligned} \tag{125}$$

which are similar to the functions $L^1_{m,n}(x, y)$. Introducing the CBM values of the field components and applying the cell boundary mapping for the asymmetrical condensed TLM node yields

$$\begin{bmatrix} 1 & 0 & 0 & 0 & 0 & 0 & 0 & 0 & 0 & 0 & -1 & 0\\ 0 & 0 & 1 & 0 & 0 & -1 & 0 & 0 & 0 & 0 & 0 & 0\\ 0 & 0 & 0 & 0 & 0 & 0 & 0 & 1 & -1 & 0 & 0 & 0\\ 0 & 1 & 0 & 0 & 0 & 0 & -1 & 0 & 0 & 0 & 0 & 0\\ 0 & 0 & 0 & 1 & 0 & 0 & 0 & 0 & 0 & 1 & 0 & 0\\ 0 & 0 & 0 & 0 & 1 & 0 & 0 & 0 & 0 & 0 & 0 & -1 \end{bmatrix} |b\rangle =$$
$$\begin{bmatrix} -1 & 0 & 0 & 0 & 0 & 0 & 0 & 0 & 0 & 0 & 1 & 0\\ 0 & 0 & -1 & 0 & 0 & 1 & 0 & 0 & 0 & 0 & 0 & 0\\ 0 & 0 & 0 & 0 & 0 & 0 & 0 & -1 & 1 & 0 & 0 & 0\\ 0 & 1 & 0 & 0 & 0 & 0 & -1 & 0 & 0 & 0 & 0 & 0\\ 0 & 0 & 0 & 1 & 0 & 0 & 0 & 0 & 0 & 1 & 0 & 0\\ 0 & 0 & 0 & 0 & 1 & 0 & 0 & 0 & 0 & 0 & 0 & -1 \end{bmatrix} \boldsymbol{T}\,|a\rangle. \tag{126}$$

Equations (124) and (126) represent twelve discretized field equations for wave amplitudes, which may be written in the form

$$|b\rangle = \boldsymbol{T}\boldsymbol{S}\,|a\rangle. \tag{127}$$

The scattering matrix $\boldsymbol{S}$ of the asymmetrical condensed node in symmetrical notation is given by (128), shown at the bottom of the page.

B. The Dispersion Analysis

For the dispersion analysis, we proceed as demonstrated in the previous sections. Eliminating the scattered wave amplitudes yields

$$(\boldsymbol{\Gamma} \quad \boldsymbol{S} \quad \boldsymbol{T} - \mathbf{1})\,|a\rangle = 0, \tag{129}$$

which implies

$$\det(\overline{\boldsymbol{\Gamma}} \quad \boldsymbol{S} - e^{j\Omega}) = 0 \tag{130}$$

in frequency and wave vector domain assuming plane wave propagation. The connection operator in wave vector domain is given by

$$\begin{aligned}\overline{\boldsymbol{\Gamma}} = {} & e^{-j\chi}(\boldsymbol{\Delta}_{1,2} + \boldsymbol{\Delta}_{3,4}) + e^{j\chi}(\boldsymbol{\Delta}_{2,1} + \boldsymbol{\Delta}_{4,3}) \\ & + e^{-j\eta}(\boldsymbol{\Delta}_{5,6} + \boldsymbol{\Delta}_{7,8}) + e^{j\eta}(\boldsymbol{\Delta}_{6,5} + \boldsymbol{\Delta}_{8,7}) \\ & + e^{-j\xi}(\boldsymbol{\Delta}_{9,10} + \boldsymbol{\Delta}_{11,12}) \\ & + e^{j\xi}(\boldsymbol{\Delta}_{10,9} + \boldsymbol{\Delta}_{12,11}).\end{aligned} \tag{131}$$

For the eigenvalues $\lambda_i = e^{j\Omega_i}$, we obtain

$$\begin{aligned}\lambda_{1,2} &= C_3 \pm \sqrt{(C_3)^2 - 1} \\ \lambda_{3,4} &= C_4 \pm \sqrt{(C_4)^2 - 1} \\ \lambda_5 &= 1 \\ \lambda_6 &= -1\end{aligned} \tag{132}$$

with

$$\begin{aligned}C_3 &= A + \sqrt{A^2 + 1/7} \\ C_4 &= A - \sqrt{A^2 + 1/7}\end{aligned} \tag{133}$$

and

$$A = \tfrac{1}{7}[\cos(\chi) + \cos(\eta) + \cos(\xi)]. \tag{134}$$

The eigenvalues λ_7 to λ_{12} are identical with λ_1 to λ_6. The eigenvalue λ_6 has an unphysical eigenvector describing an oscillating, stationary solution, the eigenvalue λ_5 represents the electromagnetic and magnetostatic case, respectively. The eigenvectors corresponding to the eigenvalues λ_1 to λ_4 describe the propagating solutions of the TLM scheme. We calculate the dispersion relation for these eigenvectors from (132) as

$$\begin{aligned}\cos(\Omega) = {} & \tfrac{1}{7}(\cos(\chi) + \cos(\eta) + \cos(\xi) \\ & + \sqrt{[\cos(\chi) + \cos(\eta) + \cos(\xi)]^2 + 7})\end{aligned} \tag{135}$$

for the eigenvalues $\lambda_{1,2}$ and as

$$\begin{aligned}\cos(\Omega) = {} & \tfrac{1}{7}(\cos(\chi) + \cos(\eta) + \cos(\xi) \\ & - \sqrt{[\cos(\chi) + \cos(\eta) + \cos(\xi)]^2 + 7})\end{aligned} \tag{136}$$

for the eigenvalues $\lambda_{3,4}$. For small arguments, using $\cos x \approx 1 - x^2/2$ and $\sqrt{1-x} \approx 1 - x/2$, (137) yields

$$4\frac{\Delta t^2}{\Delta l^2}\omega^2 = {k_x}^2 + {k_y}^2 + {k_z}^2 \tag{137}$$

which is identical with the dispersion relation of a three-dimensional wave equation with the wave propagation velocity $c = c_m/2$. The dispersion relation of $\lambda_{3,4}$ has no solution for $\Omega = 0$ but a solution for $\Omega = \pi$. We use $\cos(x + \Pi \approx -1 + x^2/2$ and $\sqrt{1-x} \approx 1 - x/2$ to approximate (136). Again, we obtain (137). The unphysical eigenvectors with $\Omega \approx \pi$ and $[\chi, \eta, \xi]^T \approx [\pi, \pi, \pi]^T$ have the same propagation characteristics as the physical eigenvectors with $\Omega \approx 0$ and $[\chi, \eta, \xi]^T \approx [0, 0, 0]^T$. However, using an excitation with a frequency spectrum bounded sufficiently below $f = 1/(2\Delta t)$, the solutions described by the unphysical eigenvectors will not be excited and thus, they will not affect the accuracy of the field computation. As for FDTD and TLM with expanded node, there are only physical eigenvectors for frequencies approaching zero.

For the calculation of the cutoff frequencies, we proceed as demonstrated for the FDTD method. For wave propagation in (1, 0, 0) direction, we have $\eta = 0$ and $\xi = 0$ yielding

$$\left|\frac{7\cos^2\Omega - 4\cos\Omega - 1}{2\cos\Omega}\right| \le 1 \quad \text{and} \quad f_c \approx 0.1579\frac{1}{\Delta t} \tag{138}$$

for the cutoff frequency f_c. For wave propagation in (1, 1, 1) direction, we have $\chi = \eta = \xi$ yielding

$$\left|\frac{7\cos^2\Omega - 1}{6\cos\Omega}\right| \le 1 \quad \text{and} \quad f_c \approx 0.2272\frac{1}{\Delta t}. \tag{139}$$

$$\boldsymbol{S} = \tfrac{1}{7}\cdot\begin{bmatrix} -2 & 2 & -1 & 0 & 2 & -1 & 2 & -1 & -1 & 0 & 5 & 2 \\ 2 & 2 & 0 & -1 & 1 & 0 & -5 & 2 & 2 & 1 & 2 & 1 \\ -1 & 0 & -2 & 2 & 2 & 5 & 0 & 1 & 1 & -2 & -1 & 2 \\ 0 & -1 & 2 & 2 & 1 & 2 & -1 & -2 & -2 & 5 & 0 & 1 \\ 2 & 1 & 2 & 1 & 2 & 2 & 1 & 0 & 0 & -1 & 2 & -5 \\ -1 & 0 & 5 & 2 & 2 & -2 & 0 & 1 & 1 & -2 & -1 & 2 \\ 2 & -5 & 0 & -1 & 1 & 0 & 2 & 2 & 2 & 1 & 2 & 1 \\ -1 & 2 & 1 & -2 & 0 & 1 & 2 & -2 & 5 & 2 & -1 & 0 \\ -1 & 2 & 1 & -2 & 0 & 1 & 2 & 5 & -2 & 2 & -1 & 0 \\ 0 & 1 & -2 & 5 & -1 & -2 & 1 & 2 & 2 & 2 & 0 & -1 \\ 5 & 2 & -1 & 0 & 2 & -1 & 2 & -1 & -1 & 0 & -2 & 2 \\ 2 & 1 & 2 & 1 & -5 & 2 & 1 & 0 & 0 & -1 & 2 & 2 \end{bmatrix}. \tag{128}$$

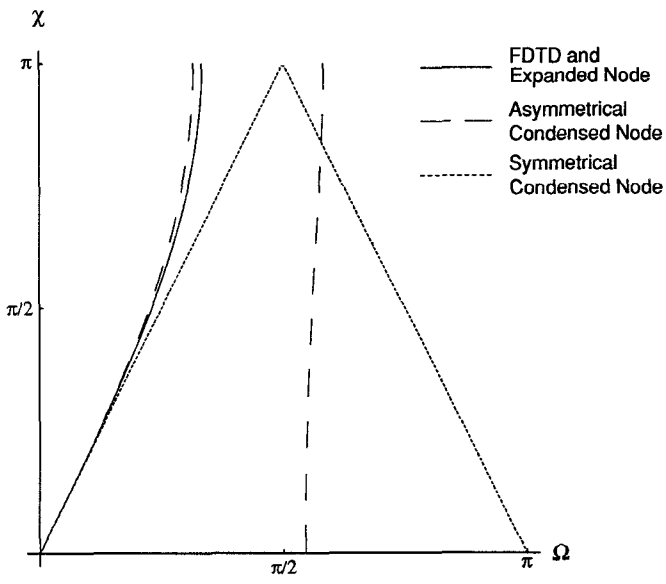

Fig. 3. Dispersion diagram for propagation in (1, 0, 0) direction.

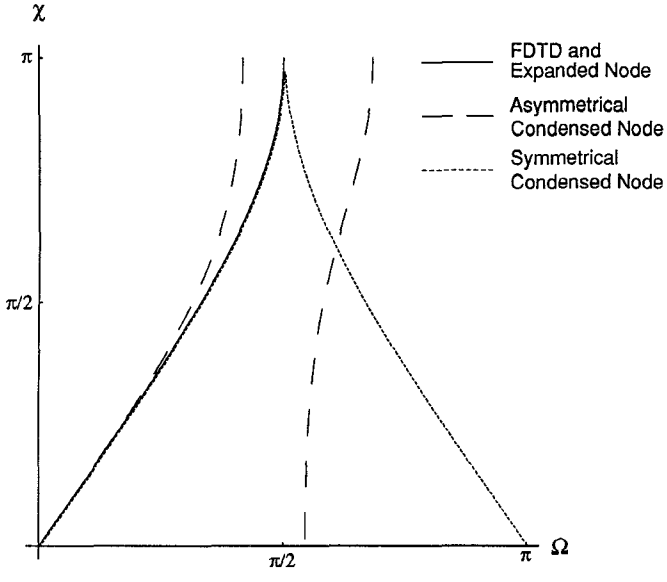

Fig. 4. Dispersion diagram for propagation in (1, 1, 0) direction.

The maximum bandwidth F of the TLM method with asymmetrical condensed node is given by $-0.1579/\Delta t \leq f \leq 0.1579/\Delta t$ and $F = 0.3158/\Delta t$, respectively.

Figs. 3–5 illustrate the dispersion characteristics of the eigenvectors describing the propagating solutions of the TLM schemes for asymmetrical condensed, expanded and symmetrical condensed node. In all three figures, there is a second branch of the dispersion curves for TLM with asymmetrical condensed node and for TLM with symmetrical condensed node which illustrates the dispersion of the unphysical eigenvectors. For the curves for TLM with symmetrical condensed node, the dispersion relation given in [10], [14] has been evaluated. For wave propagation in (1, 0, 0) direction (Fig. 3), there is no dispersion for solutions described by the eigenvectors of the symmetrical condensed node for $0 < \Omega < \pi/2$. For wave propagation along the diagonal in the x–y-plane and in (1, 1, 0) direction, respectively (Fig. 4), we have used $\chi = \eta$ and $\xi = 0$ in the evaluation of the dispersion relations. In this case, the dispersion characteristics of the eigenvectors for FDTD and TLM with expanded node, respectively, are identical with the dispersion characteristics of the eigenvectors for TLM with symmetrical condensed node for $0 < \Omega < \pi/2$. Fig. 5 illustrates the dispersion for wave propagation in (1, 1, 1) direction. The ambiguity of the physical eigenvectors for TLM with symmetrical condensed node for frequencies approaching zero [10], [14] leads to the appearance of spurious modes [19]. In general, the deviations of the dispersion relation for TLM with asymmetrical condensed node from the linear dispersion relation are larger than the deviations of the dispersion relation for FDTD and TLM with expanded node. This confirms the results for the maximum bandwidth: The maximum bandwidth of TLM with asymmetrical condensed node is smaller than the maximum bandwidth of FDTD and TLM with expanded node.

V. Conclusion

Applying the Method of Moments to Maxwell's equations, field theoretical derivations of the three-dimensional TLM method with expanded node and of the three-dimensional TLM method with asymmetrical condensed node have been given. The same approach has been used to derive Yee's FDTD method with central difference approximations. For this FDTD scheme, there are six linearly independent field components for each FDTD cell. By a dispersion analysis, we have shown that all the eigenvectors describe solutions of the FDTD scheme which converge to solutions of Maxwell's equations for frequencies approaching zero. Thus all the six FDTD eigenvectors represent physical eigenvectors. The lowest cutoff frequency f_c determining the maximum bandwidth of the FDTD method is given by $f_c = 1/(6\Delta t)$ for a stability factor $s = 1/2$ chosen identical with the stability factor of the TLM method.

Deriving the TLM method with expanded node, the field expansions of the magnetic field components are shifted by half a discretization interval in space and time with respect to the field expansions of the electric field components. Thus the series expansions for the electric and magnetic field components are similar to the series expansions for the field components of the FDTD scheme. As in FDTD, there are six linearly independent field components for each three-dimensional TLM cell. Each of these electric and magnetic field components is defined at the center of one of the six two-dimensional TLM nodes of one expanded node. To apply the cell boundary mapping and to introduce wave amplitudes, respectively, the CBM (cell boundary mean) values of the field components are introduced. The CBM values are identical with the values of the series expansions of the field components at the cell boundaries. In the derivation, we have used six relations for the CBM values of the electric and magnetic field components which are not derived from Maxwell's equations. These relations are imposed arbitrarily causing the scattering at the three shunt nodes to be shifted by half a discretization interval in space and time with respect to the scattering at the three series nodes. The relations are necessary in order to obtain all of the twenty-four discretized field equations for

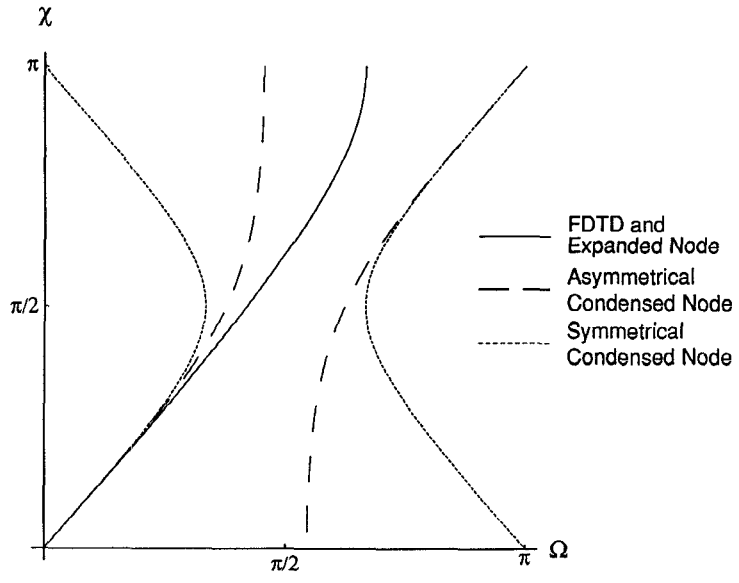

Fig. 5. Dispersion diagram for propagation in (1, 1, 1) direction.

wave amplitudes which determine the two 12×12-scattering matrices of the expanded TLM node uniquely. Due to the six additional relations, unphysical eigenvectors occur in the TLM scheme for the expanded node. Only six out of the twelve eigenvectors in the TLM scheme for the expanded node are physical eigenvectors. These physical eigenvectors have the same propagation characteristics as the FDTD eigenvectors. Thus the maximum bandwidth of TLM with expanded node is the same as for FDTD with the stability factor $s = 1/2$. The other six eigenvectors describe spurious solutions of the TLM scheme which do not exist in the FDTD scheme.

Deriving the TLM method with asymmetrical condensed node from Maxwell's equations, the six linearly independent electric and magnetic field components are defined at the center of the TLM cell. The twelve CBM values of the field components correspond to the mean values of the field components of two neighboring TLM cells. Sampling Maxwell's equations with two different sets of test functions yields twelve discretized field equations for the field components and for the wave amplitudes, respectively. As demonstrated by a dispersion analysis, sampling Maxwell's equations twice leads to unphysical eigenvectors of the TLM scheme with asymmetrical condensed node. Only six out of the twelve eigenvectors are physical eigenvectors. Compared with FDTD and TLM with expanded node, respectively, the deviations of the dispersion relation for the physical eigenvectors from the linear dispersion relation are larger leading to more dispersion in a mesh with asymmetrical condensed nodes. This results in a smaller maximum bandwidth which is determined by the lowest cutoff frequency of $f_c = 0.1579/\Delta t$.

For the three-dimensional TLM schemes investigated in this paper and in [7], twelve wave amplitudes and twelve field components, respectively, are necessary to determine the complete field state. For the TLM method with expanded node and for the TLM method with asymmetrical condensed node, only six field components are linearly independent for each TLM cell, whereas for the TLM method with symmetrical condensed node, there are twelve linearly independent field components per TLM cell. In this case, the number of wave amplitudes per TLM cell corresponds to the number of degrees of freedom per TLM cell. However, the TLM method with symmetrical condensed node exhibits disadvantages with respect to the dispersion characteristics, as there is an ambiguity of the physical eigenvectors for frequencies approaching zero [10], [14]. This ambiguity leads to the appearance of spurious modes [19]. It does not exist for FDTD and TLM with expanded and with asymmetrical condensed node.

In contrast to FDTD, half of the eigenvectors in the TLM scheme for expanded, asymmetrical condensed and symmetrical condensed node are unphysical eigenvectors. The unphysical eigenvectors describe stationary solutions oscillating with the frequency $f = 1/(2\Delta t)$ and modes approaching a frequency $f = 1/(2\Delta t)$ for wave numbers approaching zero, respectively. Using an excitation with a frequency spectrum bounded sufficiently below $f = 1/(2\Delta t)$, the solutions described by the unphysical eigenvectors will not be excited and thus, they will not affect the accuracy of the field computation. However, the fact that half of the eigenvectors are unphysical eigenvectors means that half of the field variables do not contribute for the calculation of physical solutions. Thus there is a redundancy factor of two for three-dimensional TLM. Therefore in conclusion, from the field theoretical point of view, each of the investigated three-dimensional TLM schemes exhibits disadvantages in comparison with Yee's FDTD scheme.

REFERENCES

[1] P. B. Johns and R. L. Beule, "Numerical solution of 2-dimensional scattering problems using a transmission-line method," *Proc. IEE.* vol. 118, no. 9, pp. 1203–1208, Sept. 1971.

[2] W. J. R. Hoefer, "The transmission line matrix (TLM) method," in *Numerical Techniques for Microwave and Millimeter Wave Passive Structures.* T. Itoh, Ed. New York: Wiley, 1989, ch. 8, pp. 496–591.

[3] P. B. Johns, "A symmetrical condensed node for the TLM-method," *IEEE Trans. Microwave Theory Tech.*, vol. MTT-35, no. 4, pp 370–377, Apr. 1987.

[4] R. F. Harrington, *Field Computation by Moment Methods.* Malabar, FL: Krieger, 1982.
[5] M. Krumpholz and P. Russer, "Two-dimensional FDTD and TLM," *Int. J. Numerical Modeling: Electronic Networks, Devices, and Fields,* vol. 7, no. 2, pp. 141–153, Feb. 1993.
[6] P. Russer and M. Krumpholz, "On the field theoretical derivation of the transmission line matrix method," in *Second Int. Workshop on Discrete Time Domain Modeling of Electromagnetic Fields and Networks,* Berlin, Germany, IEEE MTT/AP Joint Chap. and CAS Chap., Oct. 1993.
[7] M. Krumpholz and P. Russer, "A field theoretical derivation of TLM," *IEEE Trans. Microwave Theory and Tech.,* vol. 42, no. 9, pp. 1660–1668, Sept. 1994.
[8] P. Saguet, "The 3D transmission-line matrix method. Theory and comparison of the processes," *Int. J. Numerical Modeling: Electronic Networks, Devices, and Fields,* vol. 2, pp. 191–201, 1989.
[9] K. S. Yee, "Numerical solution of initial boundary value problems involving Maxwell's equations in isotropic media," *IEEE Trans. Antennas Propagat.,* vol. AP-14, no. 3, pp. 302–307, May 1966.
[10] M. Krumpholz and P. Russer, "On the dispersion in TLM and FDTD," *IEEE Trans. Microwave Theory Tech.,* vol. 42, no. 7, pp. 1275–1279, July 1994.
[11] L. N. Trefethen, "Group velocity in finite difference schemes," *SIAM Rev.,* vol. 24, no. 2, Apr. 1982.
[12] D. R. Lynch and K. D. Paulsen, "Origin of vector parasites in numerical Maxwell solution," *IEEE Trans. Microwave Theory Tech.,* vol. 39, no. 3, pp. 383–394, Mar. 1991.
[13] J. Nielsen and W. J. R. Hoefer, "Generalized dispersion analysis and spurious modes of 2-D and 3-D TLM formulations," *IEEE Trans. Microwave Theory Tech.,* vol 41, no. 8, pp. 1375–1384, Aug. 1993.
[14] M. Krumpholz and P. Russer, "A generalized method for the calculation of TLM dispersion relations," in *EMC 1993,* Madrid, Spain, Sept. 1993, pp. 288–291.
[15] P. Russer and M. Krumpholz, "The Hilbert space formulation of the TLM method," *Int. J. Numerical Modeling: Electronic Networks, Devices and Fields,* vol. 6, no. 1, pp. 29–45, Feb. 1993.
[16] J. C. Strikwerda, *Finite Difference Schemes and Partial Differential Equations.* Pacific Grove, CA: Wadsworth & Brooks, 1989.
[17] K. E. Gustafson, *Partial Differential Equations and Hilbert Space Methods,* 2nd ed. New York: Wiley, 1987, p. 176.
[18] M. Krumpholz and P. Russer, "Discrete time-domain Green's functions for three-dimensional TLM modeling of the radiating boundary conditions," in *ACES 1993,* Monterey, CA, Mar. 1993, pp. 458–466.
[19] J. Nielsen, "Spurious modes of the TLM condensed node formulation," *IEEE Microwave and Guided Wave Lett.,* vol. 1, no. 8, pp. 201–203, Aug. 1991.

Michael Krumpholz (M'95), for a photograph and biography, see this issue, p. 1934.

Christian Huber, for a photograph and biography, see this issue, p. 1934.

Peter Russer (SM'81–F'94), for a photograph and biography, see this issue, p. 1934.